6-1-2022

Understanding Rapid Intercalation Materials One Parameter at a Time

Wessel van den Bergh

Morgan Stefik
University of South Carolina, stefik@mailbox.sc.edu

Publication Info

Published in *Advanced Functional Materials*, Volume 32, Issue 31, 2022.

Additive Manufacturing: Metallurgy, Cut Analysis & Porosity

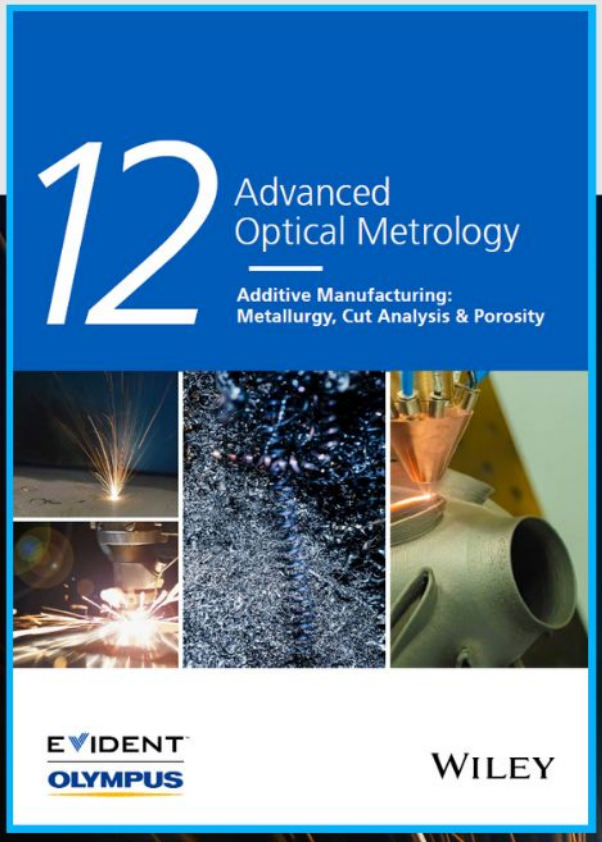

The latest eBook from Advanced Optical Metrology. Download for free.

In industry, sector after sector is moving away from conventional production methods to additive manufacturing, a technology that has been recommended for substantial research investment.

Download the latest eBook to read about the applications, trends, opportunities, and challenges around this process, and how it has been adapted to different industrial sectors.

EVIDENT
OLYMPUS

WILEY

ADVANCED FUNCTIONAL MATERIALS
www.afm-journal.de

Understanding Rapid Intercalation Materials One Parameter at a Time

*Wessel van den Bergh and Morgan Stefik**

Demand for fast, energy-dense storage drives the research into nanoscale intercalation materials. Nanomaterials accelerate kinetics and can modify reaction path thermodynamics, intercalant solubility, and reversibility. The discovery of intercalation pseudocapacitance has opened questions about their fundamental operating principles. For example, are their capacitor-like current responses caused by storing energy in special near-surface regions or rather is this response due to normal intercalation limited by a slower faradaic surface-reaction? This review highlights emerging methods combining tailored nanomaterials with the process of elimination to disambiguate cause-and-effect at the nanoscale. This method is applied to multiple intercalation pseudocapacitive materials showing that the timescales exhibiting surface-limited kinetics depended on the total intercalation length scale. These trends are inconsistent with the near-surface perspective. A revised current-model without assuming special near-surface storage fits experimental data better across wide timescales. This model, combined with tailored nanomaterials and the process of elimination, can isolate material-specific effects such as how amorphization/defect-tailoring modifies both insertion and diffusion kinetics. Avenues for both faster intercalation pseudocapacitance and increased energy density are discussed. A relaxation time argument is suggested to explain the continuum between battery-like and pseudocapacitive behaviors. Future directions include synthetic methods emphasizing tailored defects and analytical methods that minimize assumptions.

1. Nanoscale Effects

Consumer and ecological pressures have increased the demand for implementation of advanced electrochemical energy storage systems. The corresponding rate of transition from mature technologies such as internal combustion engines to battery-powered drivetrains in automobiles continues to accelerate.[1,2] The US Department of Energy predicts that annual sales of passenger electric vehicles will increase tenfold (>50 million) in <20 years.[3] The ability to rapidly charge electrical energy storage systems is particularly critical for vehicle and consumer electronic applications to minimize wait times and improve market adoption.[4,5] Correspondingly, the development of new electrochemical materials with accelerated (dis)charge kinetics are a subject of intense research. Nanoscale materials open up opportunities for several advantages including accelerated diffusion processes and enhanced specific surface area in addition to novel properties that are not observed at larger length scales and go beyond simple dimensional changes.[6] For example the Li_xCoO_2[7,8] cathode material in the first commercial secondary (rechargeable) Li-ion battery,[9] was later found to markedly change with nanoscaling. The decreased particle size correlated to transitions in galvanostatic profile from a voltage plateau observed in materials which undergo a first-order phase transition upon lithiation to a pseudolinear response that is more typical of capacitors (**Figure 1**a). Later lithiation studies of Li_xTiO2,[10–12] Li_xFePO_4,[13–17] and $Li_xTi_5O_{12}$[18,19] nanoparticles suggested that the suppression of first order phase changes was responsible for the deformation and loss of the voltage plateau observed in galvanostatic measurements. First order phase changes tend to result in voltage plateaus as the boundary between the lithium-poor and lithium-rich regions moves across the material. However, these phase transitions require energy, resulting in voltage offsets between anodic and cathodic cycles where this hysteresis reduces overall energy efficiency. For example, separation into lithium-poor phases, such as olivine α-Li_xFePO_4[16] or $Li_{0.03}TiO_2$,[11] from lithium-rich phases such as olivine β-Li_xFePO_4[16] or $Li_{0.5}TiO_2$,[11] depend upon the solubility limits of the respective phases (Figure 1b). Importantly, these solubility limits have been shown to vary significantly with particle size where such first order phase changes can be fully suppressed by nanostructuring, resulting in solid solution behavior. For example, TiO_2 particles <7 nm accommodate up to $Li_{0.22}TiO_2$[11] which was attributed to the high strain energy that would be associated with subsequent phase separation from lithiation stress.[20] Such relationships of crystal size to lithiation-induced strain/stress also have ramifications for battery longevity where, for example, Li_xCoO_2 particles below 300 nm are more resistant to fracturing which otherwise decreases battery capacity with repeated cycling.[21] This same relationship has driven the design

W. van den Bergh, M. Stefik
Department of Chemistry and Biochemistry
University of South Carolina
Columbia, SC 29208, USA
E-mail: morgan@stefikgroup.com

The ORCID identification number(s) for the author(s) of this article can be found under https://doi.org/10.1002/adfm.202204126.

DOI: 10.1002/adfm.202204126

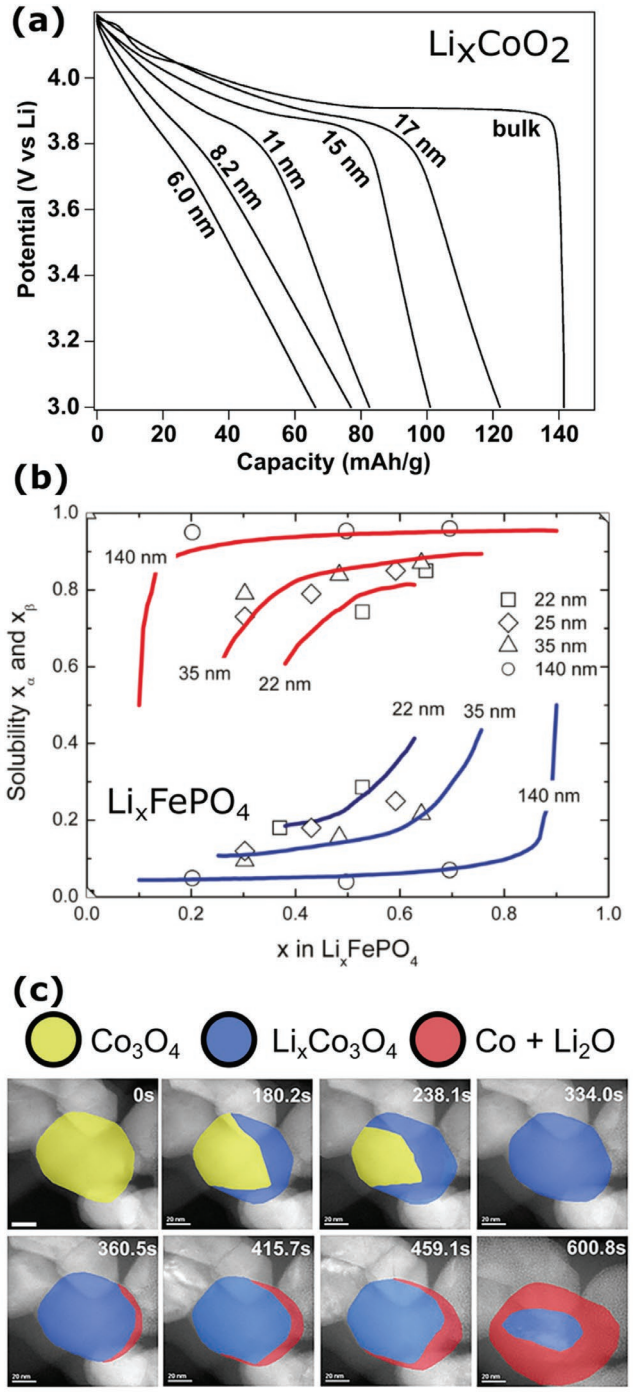

Figure 1. a) Discharge curves for crystalline Li_xCoO_2 as a function of particle size where there is a transition from a battery-like voltage plateau to a pseudolinear capacitor-like response with decreasing size. Adapted with permission.[8] Copyright 2007, American Chemical Society. b) Solubility limits for olivine Li_xFePO_4 (blue, Li-poor) α-phase and (red, Li-rich) β-phase monotonically converge with decreasing particle size. Adapted with permission.[16] Copyright 2011, American Chemical Society. c) High surface area and short diffusion paths of nanoscale design mediate more uniform phase changes from pristine Co_3O_4 (yellow) to intermediate $Li_xCo_3O_4$ (blue) and finally conversion to metallic Co and Li_2O (red). Adapted with permission.[25] Copyright 2016, American Chemical Society.

of nanoscale silicon anodes[22] which involve an alloying-mechanism with significant >230% volumetric expansion upon lithiation[23] that results in cracking and poor coulombic efficiency if the feature sizes are too large and without free-volume. Nanostructuring Si improves the accommodation of volumetric changes while minimizing lithiation strain, enabling 92% capacity retention after 700 cycles.[24] Nanoscaled materials can also increase lithiation reversibility for multiple mechanisms. For example, Co_3O_4 transitions from a conversion material which lithiates via the formation of metallic Co and Li_2O, to an intercalation material upon nanoscaling. Here nanoscaling avoids inhomogeneous phase changes and reduces the volumetric expansion, reducing fracturing, and enhancing capacity retention (Figure 1c).[25,26] For example, Li_xFePO_4 intercalates lithium via 1D channels that are sensitive to antisite defects of interstitial Fe atoms that block lithium-ion diffusion where nanostructuring reduces the 1D channel length to enhance lithium transport.[27–29] Theory has also contributed to the understanding of such nanoscale lithiation phenomena. For instance, a mathematical model[30] characterizing fracturing in the cathode material $Li_xMn_2O_4$, distinguished stress from lithium intercalation depended upon (dis)charge rate, particle size, and solid-state diffusivity while stress from phase transitions is dependent upon the ratio of phases. Recent works have examined lithiation stress heterogeneity[31,32] and nanomaterial morphologies that better accommodate this stress.[24,33–37] It is worth pausing for a moment to address a notion often expressed about nanomaterials in that they are associated with low tap densities and reduced stability owing to side reactions,[6,38] for example, excessive solid electrolyte interface (SEI) formation. From another perspective, these are rather material challenges that lead to excessive additive content (carbon/binder).[39] For example, carbon additives would not be necessary if the active materials themselves were more electrically conductive.[38] Similarly, binder additives are needed to hold nanoparticles together but would not be necessary if the nanomaterial was prepared as a continuous porous solid. In other words, high tap density is possible by minimizing the volume fraction of non-active material (porosity/electrolyte and additives) and is not fundamentally limited by using nanomaterials. For example, recent niobates exhibit negligible SEI formation[40] due to the operating voltage and have demonstrated remarkably high tap densities.[38] The horizon for nanoscale electrical energy storage materials is bright where accelerated charging occurs with reduced transport lengths, suppression of first order phase transitions improves kinetics and reversibility, and better strain accommodation enhances cycling stability.

2. Rapid Intercalation Materials and Pseudocapacitance

The development of rapid intercalation materials led to the discovery of intercalation pseudocapacitance. Pseudocapacitance was first conceptualized by Conway in 1962[41] where an essential attribute is a capacitor-like response, for example, having the current (i) proportional to the voltage sweep rate (ν). Current relationships with ν are often expressed as a power law:[42]

$$i = a\nu^b \quad (1)$$

where a and b are fit terms and $b = 1.0$ for an ideal capacitor. As the term "pseudo" (meaning fake) implies, pseudocapacitive responses should not be associated with classic double layer charging as in an electric double layer capacitor (EDLC) but are rather associated with faradaic surface charge transfer processes. A series of seminal works on RuO_2,[43,44] MnO_2,[45] TiO_2(B),[46,47] V_2O_5,[48] α-MoO_3,[49] and T-Nb_2O_5,[50,51] raised considerable excitement for the potential of such rapid current responses. The cyclic voltammetry (CV) characteristics of these materials fall broadly into two camps,[52,53] 1) surface redox pseudocapacitance which has dominant box-like character (RuO_2, MnO_2) (**Figure 2**a) and 2) intercalation pseudocapacitance which has dominant peak-like character (TiO_2(B), V_2O_5, α-MoO_3, T-Nb_2O_5) (Figure 2b). There is debate about the fundamental nature of these responses,[52,54–61] including rigorous theoretical arguments that the first camp is attributed principally to EDLC[60] and a separate suggestion of a continuum between Faradaic and EDLC.[62] If indeed charge storage were dominated by EDLC, then the term pseudocapacitance[60] would be inaccurate. T-Nb_2O_5 was the first material described as exhibiting intercalation pseudocapacitance.[51] With intercalation pseudocapacitance, as the name implies, charge storage dominantly proceeds by faradaic reactions throughout the extent of the solid via intercalation. Naturally this behavior requires sufficiently rapid diffusion to observe capacitor-like kinetics (surface-limited, Equation (1) with $b \approx 1.0$). In contrast, the term "batteries" and generally other intercalation materials are often associated with diffusion limitations (Equation (1) with $b = 0.5$ for semi-infinite diffusion).

A range of definitions for pseudocapacitance have been proposed. Many definitions include faradaic reactions, reversibility (e.g., mirror like CV profiles), and a lack of diffusion limitations, that is, surface-limited kinetics.[52,54–57,61] We support this generally agreed upon and broadest definition. Costentin has argued that "pseudocapacitance" is an incorrect notion where such reported box-like (redox pseudocapacitive) CV curves should be interpreted as EDLC and peak-like (intercalation pseudocapacitive) curves should be interpreted as normal battery-like intercalation undergoing slow charge transfer or ohmic drop.[60,63] That latter interpretation, however, is compatible with the broad definition above for intercalation pseudocapacitance where the question should become whether this behavior is worthy of a special name "intercalation pseudocapacitance." We thus continue to use the term intercalation pseudocapacitance here. Others have extended the pseudocapacitance definition to be further constrained to examples exhibiting a linear relationship between the applied potential and the state of charge such as RuO_2 (Figure 2a).[64] Elsewhere it was suggested that the broader definition include pseudolinear relationships between the applied potential and the state of charge such as T-Nb_2O_5.[52,53,55] The distinction between intercalation pseudocapacitance (pseudolinear) and battery-like behavior (plateau) notably can become blurred with nanostructured materials.[53,65] Nanostructured intercalation materials can depart from the localized and well-defined intercalation potentials of batteries where intercalation pseudocapacitance exhibits broadened CV peaks with a delocalized[66] distribution of potentials that have been rationalized in terms of concentration dependent activity coefficients.[59] Typical quantitative

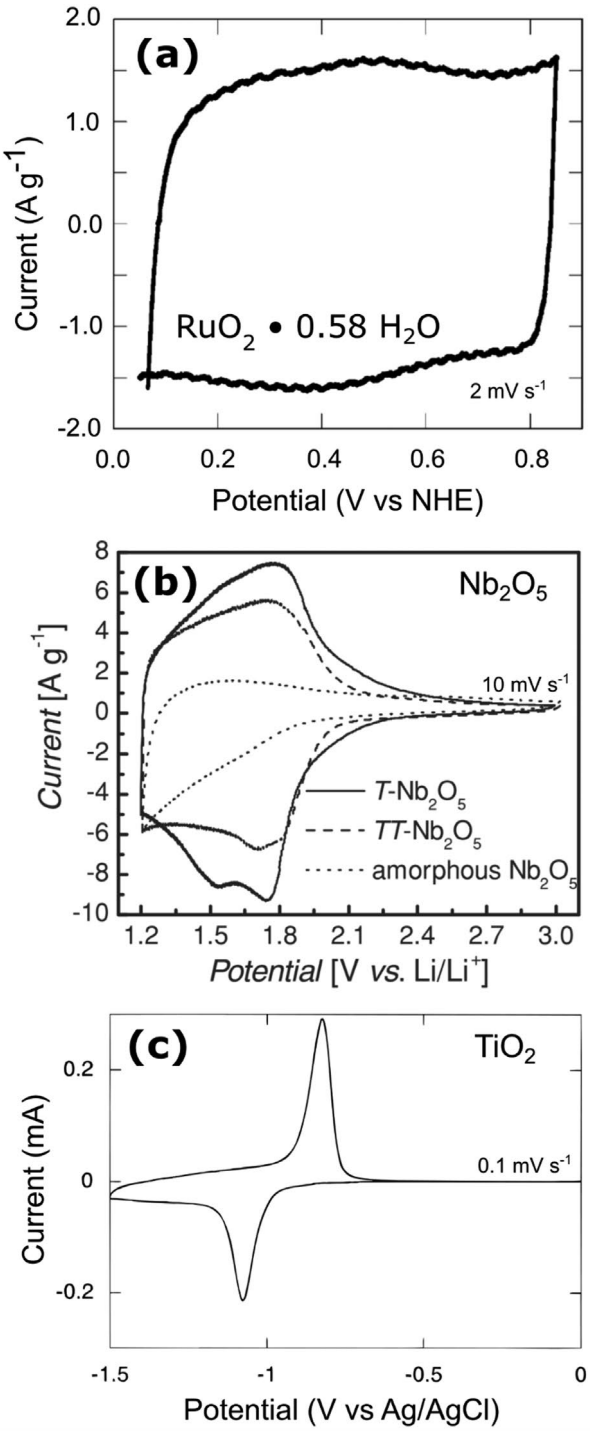

Figure 2. a) RuO_2 exhibits a box-like CV response corresponding to its typical labelling as a surface redox pseudocapacitive material. Adapted with permission.[64] Copyright 2002, American Chemical Society. b) T-Nb_2O_5 exhibits a peak-like and mirrored CV response corresponding to its labeling as an intercalation pseudocapacitive material. Adapted with permission.[75] Copyright 2011, WILEY-VCH Verlag GmbH & Co. KGaA, Weinheim. c) In contrast, typical battery-like materials such as anatase TiO_2 exhibit peak separation at all ν (not mirrored) corresponding to energy loss to, for example, first order phase changes. Adapted with permission.[42] Copyright 1997, American Chemical Society.

metrics used to identify surface-limited pseudocapacitive responses include $i \propto \nu$ in CV (Equation (1) with $b \approx 1.0$) or a phase angle of ≈90° in electrochemical impedance spectroscopy (EIS). Others have further delineated that pseudocapacitors should not exhibit diffusion-limitations on the minute timescale or above.[55] It will take time for practitioners in this field to agree upon definitions which in part have been limited by the present state of understanding.

3. Open Questions

Several aspects of T-Nb_2O_5 lithiation have ambiguous or contested interpretations in recent years. Intrinsic properties are generally defined as being inherent to a material itself without need for external modifications such as length scale control. The suggested notions of extrinsic versus intrinsic pseudocapacitive materials were intended to distinguish between materials depending on whether they require feature size control to exhibit pseudocapacitive characteristics.[57] This distinction has however gradually blurred over time from an initial notion consistent with the definition of "intrinsic"[57,67] (independent of length scale) to a generalization of "a wide range of length scales."[51,55,68] For example, some have argued that intercalation pseudocapacitance in T-Nb_2O_5 is an intrinsic property.[57] This assignment appears to conflict with an initial study by Bard et. al.[69] where lithiation exhibited a plateau-like state of charge response (25 h delithiation) and had limited reversibility for the micron scale materials investigated. Neither of these attributes are consistent with typical pseudocapacitance characteristics.[51] Similarly a recent study of micron scale T-Nb_2O_5 identified polarization constraints at rates >3C,[70] again not consistent with intrinsic pseudocapacitance. Here C-rate is defined inversely with the theoretical number of times a battery could be (dis)charged in an hour, for example, 10C-rate corresponds to a 1/10 h or 6 min (dis)charge time. Others have reported similar non-pseudocapacitive responses for T-Nb_2O_5 such as large capacity reductions at modest charge rates[71] or a plateau-like state of charge responses.[72] The only other material described as being an intrinsic intercalation pseudocapacitor is bronze-TiO_2[52,61] which has principally been investigated as nanoscale materials with conductive additives to make up for its low electronic conductivity.[73] For example, bronze-TiO_2 can exhibit significant capacity loss at rates of just 1C[74] which is not consistent with an intrinsic absence of diffusion limitations. The fundamental dependence of intercalation pseudocapacitance upon transport processes with length scale dependencies naturally limits the material dimensions[39] before, for example, transport constraints prevent realization of mirror-like CV profiles. Given these fundamental kinetic dependencies, it seems that the notion of intrinsic intercalation pseudocapacitance is not substantiated. Furthermore, there is need for an expanded theoretical understanding of length scale dependent changes in electrochemical character. For example, a linear state of charge voltage response may require that the charge rate does not exceed the rate of electronic/ionic communication across the active material. The mechanistic perspective of intercalation pseudocapacitance in T-Nb_2O_5 (and others) is another topic of debate. Are their capacitor-like current responses caused by storing energy in a special near-surface region[57,75] or rather is this response due to normal intercalation limited by a slower faradaic surface-reaction[39,63] or other non-idealities? The former perspective assumes that the current comes from two distinct zones including a special near-surface zone operating with surface-limited kinetics and an interior zone operating with diffusion-limited kinetics. The summative current model associated with this perspective was first proposed by Conway for modeling the current response of surface redox pseudocapacitance from molybdenum nitride[76]

$$i = k_1\nu + k_2\nu^{0.5} \text{ "parallel model"} \quad (2)$$

where k_1 and k_2 are fit terms. This model is equivalent to a parallel circuit with two pathways for current contributing independently, termed here as the "parallel model" (**Figure 3**). CV current-responses interpreted mechanistically with the parallel model associate a portion of the current (and a thus portion of the charge stored) with a capacitive, near-surface region, and a separate portion of the current (and a portion of the charge stored) with intercalation. This model predicts a fixed depth of the near surface region which is invariant with electrode dimensions. The parallel model in this context has met with criticism.[59,60,63,77] Another perspective is that intercalation pseudocapacitance operates by charge storage via normal intercalation with additional rate-controlling processes such as a surface-limited faradaic reaction or ohmic drop in the pores.[63,78–80] As more rapid intercalation processes are discovered it is expected that other processes may increasingly become rate limiting.[39] This perspective is equivalent to a series circuit with two (or more) rate-dependent processes which all impede the overall rate as a collective (Figure 3).[78] A corresponding $i(\nu)$ equation for the "series model" is explained later in detail. This series perspective predicts that the intercalation length scale contributes to the rate-dependence of the current response. As discussed more later, the parallel model and series model also make markedly different predictions for b-value(ν). Numerous experimental datasets show that the Equation (1) power-law response for T-Nb_2O_5 (and other intercalation pseudocapacitance materials) gradually transitions from surface-limited ($b = 1.0$) to lower b-values with increasing ν. The specific cause of this drop in b-value has been interpreted multiple ways, including possible diffusion limitations[51,81] for either intercalation/electrolyte transport, polarization of the surface,[82] and ohmic drop in pores.[60] Resolving these ambiguities would help advance energy storage materials by better understanding cause-and-effect. For this disambiguation it can be valuable to isolate the effects of each fundamental reaction step.

4. Ambiguity Challenge with Convolved Processes

Isolating the effects of each fundamental reaction step is challenging. Energy storage via electrochemical intercalation, including intercalation pseudocapacitance, depends on multiple diffusion/transport processes (intercalation, electrolyte transport, electron transport) and surface processes.[39] Dozens of recent T-Nb_2O_5 investigations using nanoparticles,[75,83–87] nanotubes,[87–90] nanorods,[91,92] nanowires,[93,94] nanosheets,[95,96]

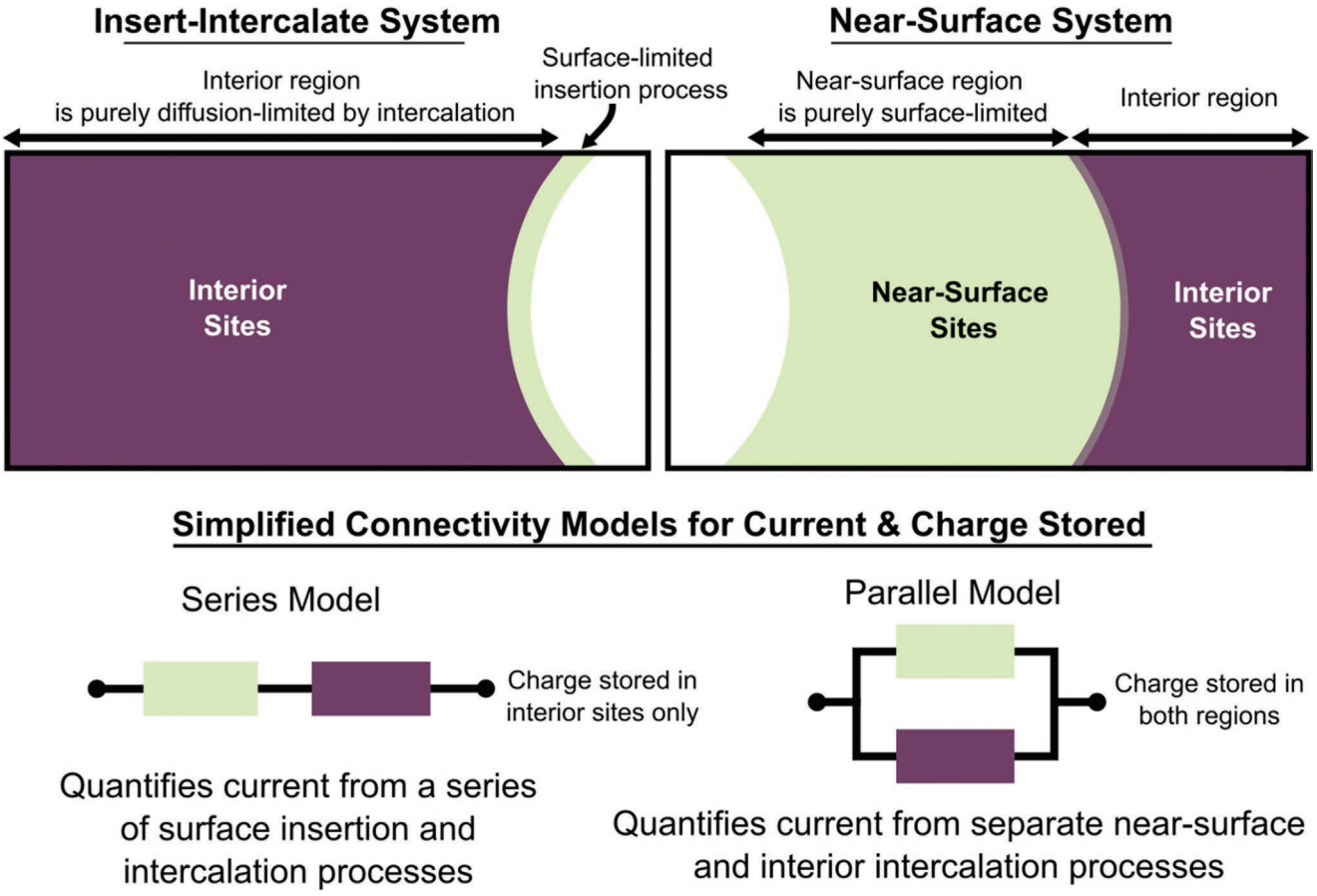

Figure 3. A comparison of the models proposed for intercalation pseudocapacitance. The Insert-Intercalate system proposes that intercalation pseudocapacitance stores energy via normal intercalation but has a relatively slower surface reaction (Series Model). In contrast, the Near-Surface system proposed two distinct zones including near-surface sites operating with surface-limited kinetics and interior sites with diffusion-limited kinetics where current and charge storage are independent for each region (parallel model).

nanocomposites,[97–103] and related nanostructures[71,104–114] have shown remarkable performance without isolating the effects of individual architectural parameters or individual processes to address the hypotheses above. This lack of variable minimization hampers comparisons between architectures and obfuscates hypothesis testing. Furthermore, the multiple diffusive processes occurring concomitantly have the same fundamental time-dependencies[115] that inhibit disambiguation with specificity except when additional information is known. This general challenge is now elaborated for four popular electrochemical analytical techniques: 1) CV data is often interpreted with power-law relationships[42] such as Equation (1) where $b = 1.0$ corresponds surface-limited (capacitor-like) kinetics and $b = 0.5$ corresponds to diffusion-limited (battery-like) kinetics in the semi-infinite condition. Intermediate b-values can arise from a convolution of rate limiting processes or finite diffusion. In the case of a diffusion-limited response, however, this relationship cannot ascribe the limitation to a specific diffusive process without additional information. 2) Electrochemical impedance spectroscopy (EIS) data are often interpreted using equivalent circuits. While quantitative and useful, the data are often similarly well-fitted by multiple equivalent circuits where it is sometimes not clear which circuit elements correspond to which fundamental processes.[116–125] A further limitation is that equivalent circuits do not consider non-uniform concentrations profiles for ions and electrons throughout the electrolyte and electrode.[116,123–125] 3) On the other hand, 3D-Bode analysis[81,126] of EIS data yields model independent descriptors including rate constants and onsets of diffusion-limited behavior. However, again due to the similar time dependence for all diffusive processes they are not possible to distinguish from each other without additional information. For example, a recent 3D bode analysis of T-Nb_2O_5 identified a semi-infinite diffusive constraint which was speculated to be associated with either intercalation or electrolyte ion diffusion.[81] 4) Physicochemical models[116,125,127] address the challenge of non-uniform concentration profiles, however even simple 3D geometries require a computational cluster. Furthermore, these models require input of an extensive number of known parameters which is a significant barrier for studying materials with yet unknown properties. These examples portray the difficulty of deconvolving concomitant diffusive processes in general when only measuring voltage and current responses over time. A central theme of this review is that this disambiguation challenge is better addressed when there is a series of samples which vary by a single spatial variable with the goal of identifying cause-and-effect one transport process at a time.

5. Varying One Architectural Parameter at a Time

Persistent micelle templates (PMTs)[78–80,128–131] are a synthesis platform that uniquely enables the production of series of porous nanomaterials that vary by a single spatial parameter at time and follow model predictions. PMTs rely on self-assembly, yield macroscopically homogeneous materials, and are scalable with simple solution processing. The basic PMT process is presented in **Figure 4**a. Independent feature size adjustments have eluded most self-assembly methods due to the reliance upon equilibration where free-energy minimization governs all attributes of the final structure. In contrast, PMT is based upon kinetic entrapment to sidestep the limitations of equilibrating micelles.[132,133] All but the most recent PMT literature[134,135] was recently reviewed comprehensively.[136] The material-to-template (M:T) ratio is an important parameter where increasing the amount of material precursors leads to expanded wall thickness with constant pore size and shape (Figure 4d–f). The preservation of constant morphology (isomorphic) is important to avoid changes in architecture tortuosity.[97,137–144] The validation of PMT materials is also facile using the PMT model to analyze small-angle X-ray scattering (SAXS) data (Figure 4b,c).[131,136,145] The PMT model is best-suited to micelle templated samples due to the assumed constant S structure factor term.[145] PMT-derived samples can be either bulk solids[135,146] or deposited as thin films,[78–80] for example, upon current collectors. When the precursors correspond to active materials only, then the resulting porous materials are free from the binders and carbon additives associated with slurry-based electrodes, thereby avoiding electrochemical contributions from side reactions[147,148] while enabling the measurement of fundamental descriptors of the active material behaviors. PMTs thus uniquely support electrochemical investigations by enabling simple comparative studies where the nanoscale architecture is varied one parameter at a time.

6. Probing Convolved Processes One Step at a Time

The combination of tailored architectures with the process of elimination can improve the identification of rate limiting steps and advance a mechanistic understanding. Others have suggested electrochemical routes to identify rate limiting steps based on a set of models.[149] Rather, the works highlighted in this review[78–80] seek to minimize the complexity of electrochemical models, avoiding the underlying assumptions, and rather rely simply upon cyclic voltammetry as the primary electrochemical measurement. Opportunities will be discussed later to expand this general approach with additional electrochemical and analytical techniques. As discussed above, power-law relationships[42] (Equation (1)) for CV data can identify transitions between surface-limited ($b = 1.0$) and semi-infinite diffusion-limited regimes ($b = 0.5$), but cannot identify which specific diffusion process limits the rate without additional information. These limits for b-values are analogous to well-known equations. For example Equation (1) with $b = 1.0$ is analogous to Lindström's $i(v)$ relationship[42] for EDLCs[150]

$$|i_C| = \mathrm{AC}_d v \tag{3}$$

where C_d is double-layer capacitance and A is the surface area. Furthermore Equation (1) with $b = 0.5$ is analogous to the Randles–Ševčík $i(v)$ relationship which is often applied to both electrolyte diffusion[150] and intercalation diffusion[42]

$$i = \mathrm{FAC}^* D^{0.5} v^{0.5} \left(\frac{\alpha F}{\mathrm{RT}}\right)^{0.5} \pi^{0.5} \chi(bt) \tag{4}$$

where T is absolute temperature and the remaining unspecified terms are constant for a given sample. Similarly, electron trans-

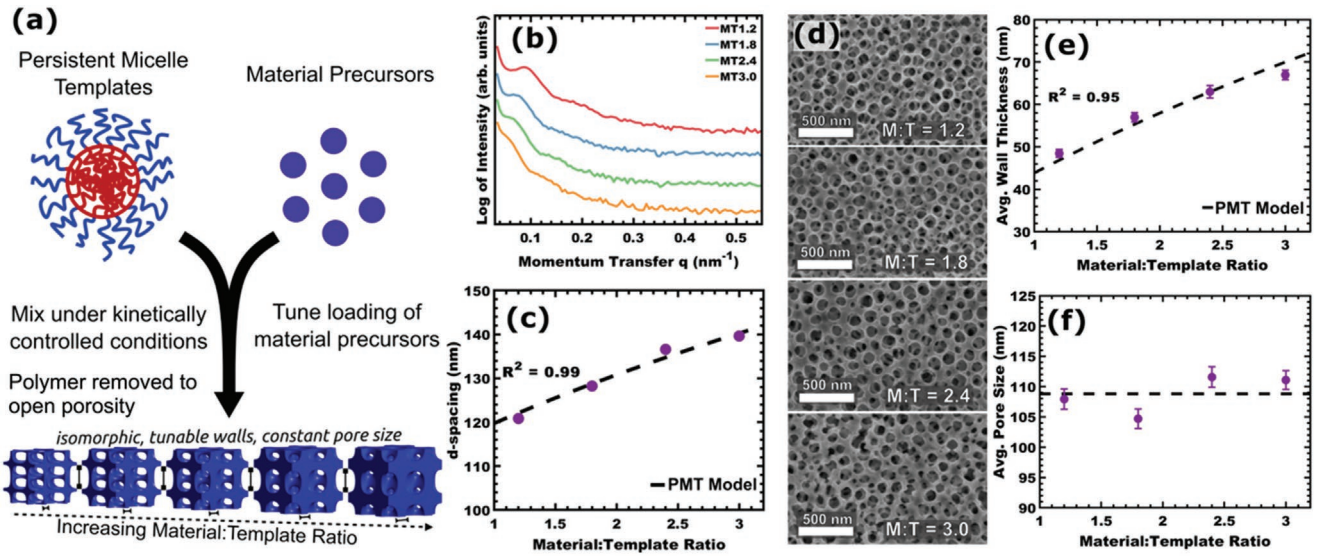

Figure 4. a) The combination of persistent micelle templates (PMTs) with material precursors leads to porous materials after removal of the micelle templates. Increasing the material-to-template (M:T) ratio increases the wall thickness while preserving constant pore size across the isomorphic sample series. b) SAXS data and the c) corresponding d-spacing ($d = 2\pi/q_{peak}$) are fitted with a PMT model. d) Measurements on SEM images of the corresponding samples yields statistically significant measures of e) average wall thickness and f) average pore size, both with respect to the PMT model. All error bars correspond to the standard error of the mean. Adapted with permission.[80] Copyright 2021, Wiley-VCH Verlag GmbH & Co. KGaA, Weinheim.

port in semiconductors is often modeled as the sum of diffusion and drift currents. Whereas the diffusion current is voltage independent and follows Fick's laws, the drift current depends on the local electric field gradient. Thus, electron transport can manifest diffusion-limited kinetics when drift current is a minority.[151] There are thus three candidate causes when CV data exhibits a diffusion-limited $i(v)$ response: electrolyte transport, intercalation transport, and electron transport. The assignment of such an observation to a specific diffusive process requires additional information. Here the availability of tailored architectures helps to reduce ambiguity. Ideally each of these three transport processes would be perturbed one a time to check for kinetic sensitivity. This approach can identify rate-limiting diffusive processes with minimal assumptions and minimal modeling.

7. Example 1: Length Scale Dependence of T-Nb_2O_5 Lithiation

As the first example, the electrochemical kinetics of a tailored series of PMT-derived T-Nb_2O_5 were examined.[80] The investigated series of T-Nb_2O_5 thin films had wall thickness ranging from 48.5–67.0 nm (M:T = 1.2–3.0) and constant pore diameter of 108.6 nm The films were measured in a three-electrode configuration against Li/Li^+ using CV over a wide range of logarithmically spaced v values (**Figure 5**a). Plotting the peak currents as $\log(i)$ versus $\log(v)$ (Figure 5b) reveals rate-dependent transitions in the type of rate limiting process based on the slope (b-value). The corresponding derivative of this plot directly shows these b-value(v) dependencies (Figure 5c). All the b-value(v) data show a transition from surface-limited kinetics to mixed kinetics and finally toward diffusion-limited kinetics with increasing v. This behavior transition was quantified using these two clearly defined b-value regimes. The departure from surface-limited kinetics at $b = 0.9$ was termed the Surface-Limited Threshold (SLT) which corresponds to the onset of diffusion-limitations. Similarly, the transition to diffusion-limited kinetics at $b = 0.6$ was termed the Diffusion-Limited Threshold (DLT) where diffusion-limitations dominate. As will be discussed in more detail in a subsequent section, the gradual decrease in b-value with increasing v is inconsistent with the parallel-model which predicts the opposite trend. Furthermore,

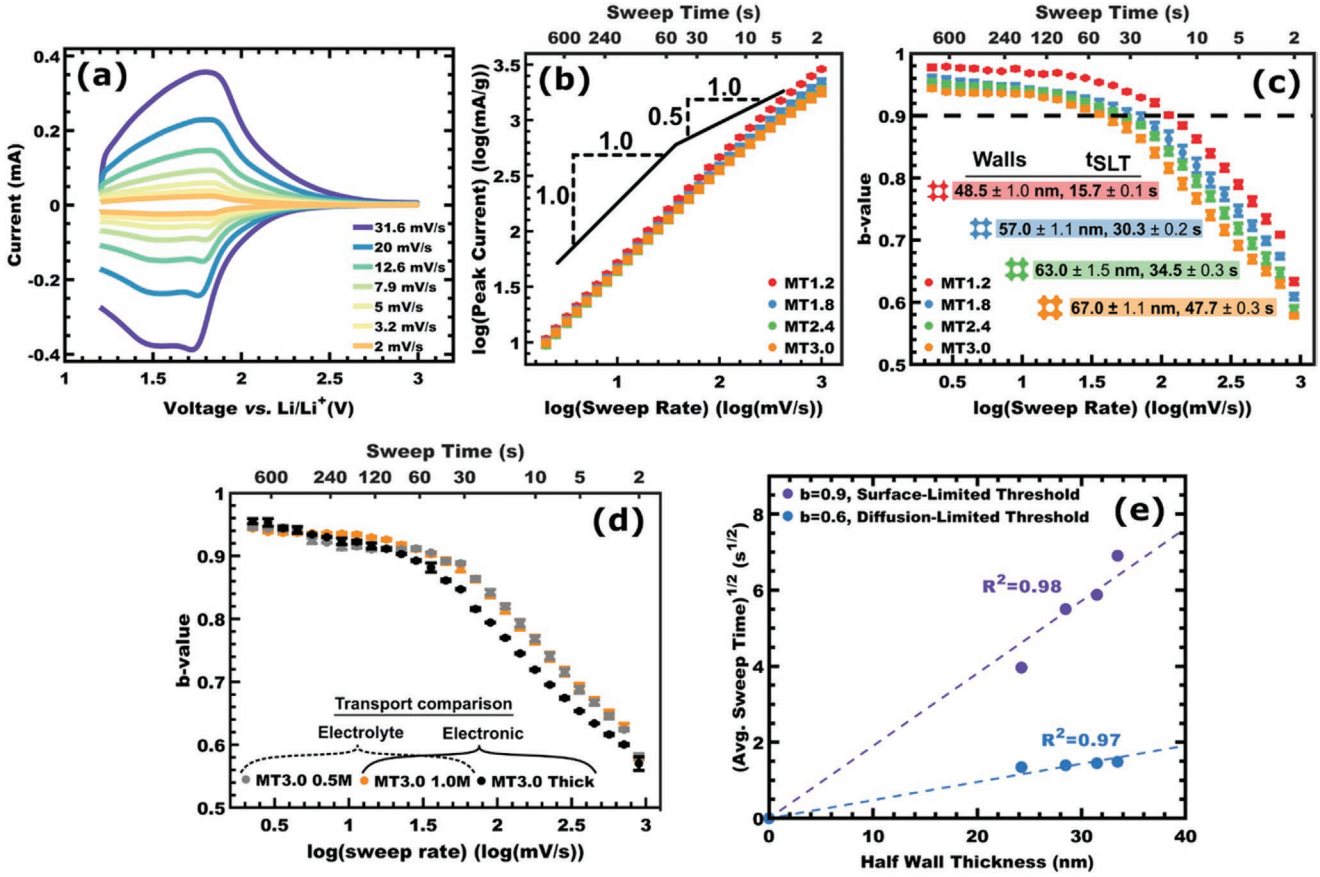

Figure 5. a) A series of T-Nb_2O_5 voltammograms collected at different v. b) A log–log plot of peak $i(v)$ identifies changes to the type of rate-limiting process based on the slope (b-value). c) The corresponding derivative shows b-value (v) changes with voltage sweep rate. The dashed line at $b = 0.9$ corresponds to the surface-limited threshold (SLT) which indicates a departure from surface-limited behavior. Systematic comparisons of c) intercalation length, d) electrolyte concentration, and d) electron transport length reveal and rank candidate transport constraints. e) Plots of $t_{SLT}^{0.5}$ and $t_{DLT}^{0.5}$ versus the intercalation pathlength (half wall thickness) are consistent with direct proportionality (dashed lines) consistent with a generalized Fick's second law solution (Equation (5)). Values are presented as a mean ± standard error-of-the-mean. Adapted with permission.[80] Copyright 2021, Wiley-VCH Verlag GmbH & Co. KGaA, Weinheim.

the general form of Figure 5c is not consistent with the expectations of the parallel model (derivative of Equation (2)) associated with a near-surface system (Figure 3), as discussed in next section. For this sample series, there was a monotonic decrease in ν_{SLT} with increasing wall thickness. For example, sample MT1.2 (48.5 nm walls) exhibited an onset of diffusion-limitations at ν_{SLT} = 114.60 ± 0.48 mV s^{-1} whereas sample MT3.0 had ν_{SLT} = 37.77 ± 0.27 mV s^{-1} which is a 3× reduction in rate. Such a large kinetic change for a minor 18.5 nm (40% rel.) change in wall thickness highlights the large effect of the extrinsic architectural changes. As explained before, further analysis was carried out to consider multiple possible sources of diffusion-limitations. First, sensitivity of the response kinetics to electrolyte transport were examined. A significant 50% reduction in $Li^+ClO_4^-$ concentration in the electrolyte was found to have no marked effect on the response kinetics for any of these samples, thus eliminating electrolyte transport as a contributor to the diffusion-limitation (Figure 5d). It is noted that the change of wall thickness is geometrically coupled with a reduction of pore/electrolyte volume fraction thus sample M:T3.0 was expected to be the most sensitive to electrolyte transport yet remained insensitive to the concentration change. Second, sensitivity of the response kinetics towards electron transport was examined. The film thicknesses were varied to modify both the electron and electrolyte transport length scales. Having excluded sensitivity of these samples toward electrolyte resistance, differences found here were attributed to electron transport alone. Increasing the film thickness by 150% resulted in 30% decrease in ν_{SLT} for sample MT3.0 (Figure 5d). In contrast, the main sample series had relatively constant film thickness ± 15%, indicating the electron transport has a minor contribution towards the overall ≈3× change in ν_{SLT}. The assignment of the dominant diffusion-limited process in these T-Nb_2O_5 films was thus assigned to the intercalation process. This process of elimination strategy is summarized in **Figure 6**. The response kinetics for diffusion-limitations are well known for the solution of Fick's second law for a semi-infinite source

$$x \propto \sqrt{Dt} \tag{5}$$

where x is the intercalation pathlength (half of the material wall thickness), D is solid-state diffusivity, and t is time. Here the sweep time was calculated by dividing the voltage window by ν. As shown in Figure 5e, the expected linear relationship between x and $t^{0.5}$ was found for the DLT (b = 0.6, t_{DLT}), consistent with the quantitative changes in wall thickness across the sample series. Furthermore, the SLT (b = 0.9, t_{SLT}), was consistent with the same scaling law. While unexpected for surface-limited kinetics alone, rather the SLT reflects a point of balance where dominant surface-limited kinetics begin to transition to diffusion-limited kinetics. From this perspective, it is anticipated that the SLT depend upon the scaling

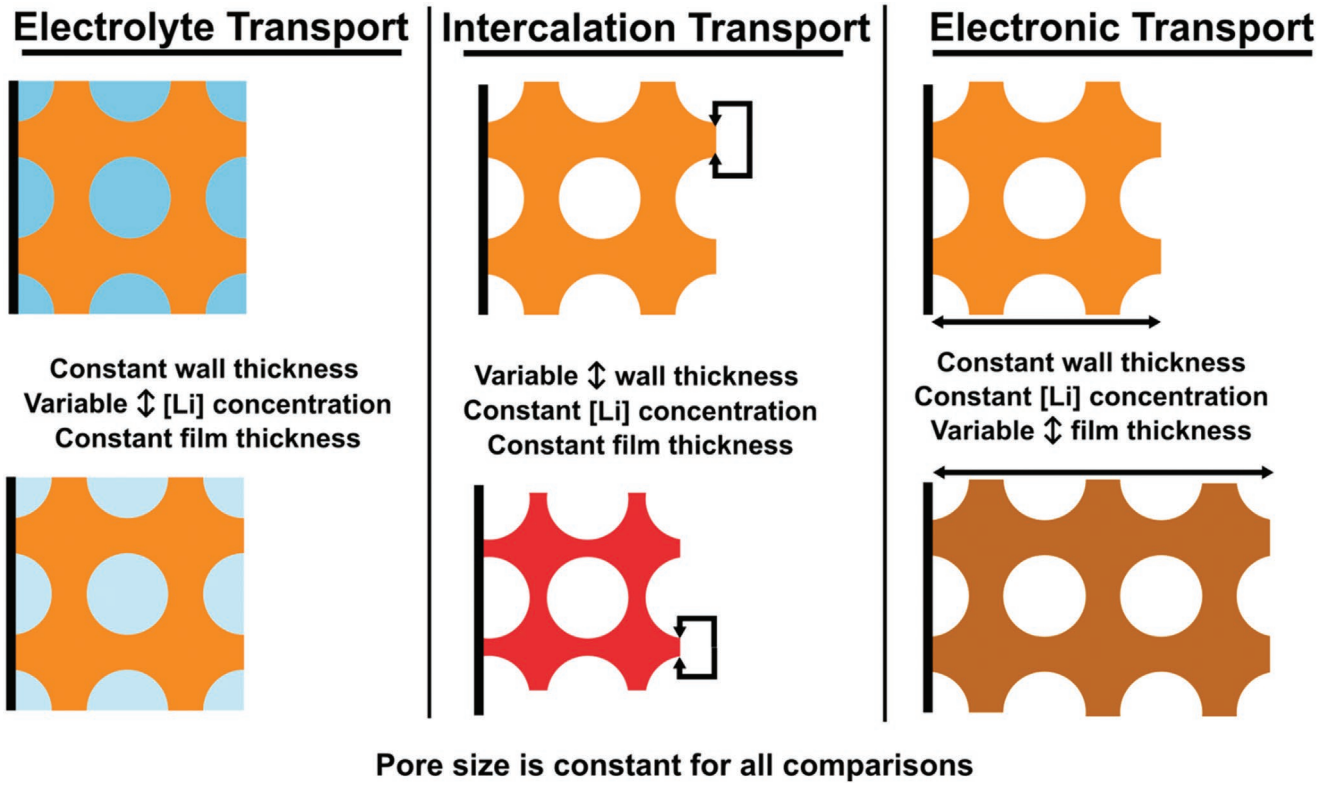

Figure 6. A process of elimination approach can identify $i(\nu)$ and b-value(ν) sensitivity to different diffusive process. Sensitivity to electrolyte transport is probed by varying the electrolyte concentration alone (left). When insensitive to perturbations in electrolyte transport then subsequent geometric variations are simpler to interpret. Sensitivity to intercalation transport is probed by varying the wall thickness alone (center). Sensitivity to electron transport is probed by varying the film thickness (right). It should be noted that both wall thickness changes and film thickness changes simultaneously modify electrolyte transport.

laws of the dominant diffusion-limited process. The fact that the timescales exhibiting surface-limited kinetics depend on the total intercalation length scale is most consistent with the series-model for intercalation pseudocapacitance via the Insert-Intercalate perspective (Figure 3). Also it is noted that the 48.5–67 nm thick walls of these samples are equivalent to ≥254–351 Nb—O bonds (1.907 angstrom/each)[152] which exceeds most notions of a "near surface" regime. This example illustrates how the combination of tailored nanomaterials with the process of elimination can disambiguate electrochemical cause-and-effect.

8. Comparison of Intercalation Pseudocapacitive Current Models

Distinct conceptual models with different scaling relationships have been proposed to understand intercalation pseudocapacitance. Here we focus on simple models with minimal terms with the motivation to identify and understand dominant electrochemical processes. Simplification naturally eliminates completeness where comprehensive models exist with a correspondingly expansive list of fit terms.[59,77,153–156] As noted above, the parallel model is consistent with two separate sources of current operating in tandem. Here the surface-limited current source is often interpreted as charge storage within a capacitive near-surface region whereas the separate diffusion-limited current source is associated with interior intercalation (Figure 3). This mathematical model has met with criticism.[59,60,63,77] A related capacity(ν) model from Trasatti[157] has also received criticism regarding the extrapolation that fails to follow data outside of a narrow sweep rate and was suggested to not be regarded as theoretically sound.[158] The basic functional form of the parallel model has two contributions with different ν-dependencies shown in **Figure 7**a. Due to the summative nature and the relative slope values this functional form necessarily predicts a transition from diffusion-limited behavior to surface-limited behavior with increasing ν. This transition is apparent in the b-value(ν) plot in Figure 7b. These $i(\nu)$ and b-value(ν) dependencies, however, are antithetical to typical data (Figure 5c). This issue is often avoided by constraining fitting to low ν to avoid polarization from, for example, diffusion limitations at high ν. When the range of experimental ν values focus on the surface-limited regime, this model often yields good fits of $i(\nu)$, however the corresponding b-value(ν) fits are poor. The resulting k_1 and k_2 values have been used to then report separately the capacitive (near-surface) and diffusion-limited (interior) currents or charge fractions which cannot be verified directly. Some have suggested that comparison to the Trasatti capacity(ν) model is a form of validation,[55,68,97,159–161] however that model invokes the same assumption of two independent charge storage mechanisms with the same kinetic dependencies and similarly fails to follow experimental data outside of a narrow ν-range. For a mechanistic model to be valuable, it should be consistent with data and enable predictions that are verifiable outside the assumptions of said model. Unfortunately, the parallel model as applied to intercalation pseudocapacitance has not yet led to verifiable predictions. For example, the relatively constant mass-normalized currents in Figure 5b with varying nanoscale architectures are not consistent with a near-surface system. A revised model was recently suggested[78] that corresponds to the Insert-Intercalate perspective (Figure 3).[78–80] This revised model thus arranges the surface and diffusion processes rather in-series where charge storage requires both processes to occur sequentially and their impedances (resistance and reactance) are additive

$$i = \left[\left(\frac{k_2}{\sqrt{\nu}}\right)^2 + \left(\frac{k_1}{\nu} + \frac{k_2}{\sqrt{\nu}}\right)^2\right]^{-0.5} \text{ "series model"} \quad (6)$$

where k_1 and k_2 here are different fit parameters analogous to impedance (lesser k values yield greater current) for surface-limited and diffusion-limited contributions respectively. An important distinction is that the series model does not separate capacitive-current from diffusive-current, rather it passes all current through both processes. Thus, the series model does not presume charge storage in a special near-surface region (Figure 3). In contrast to the parallel model, the series model transitions from surface-limited to diffusion-limited kinetics with increasing ν (Figure 7c,d). While Equation (6) was shown to fit both $i(\nu)$ data well and b-value(ν) data fair, a third term can be added to improve the latter fit. A range of third terms were screened including addition of a resistor, additional of another diffusion-limited processes, and modifying the surface-limited process to be analogous to a constant phase element. The resistor addition led to the best fits where

$$i = \left[\left(\frac{k_2}{\sqrt{\nu}} + R\right)^2 + \left(\frac{k_1}{\nu} + \frac{k_2}{\sqrt{\nu}}\right)^2\right]^{-0.5} \text{ "series model with R"} \quad (7)$$

This series model with R (Equation (7)) yields excelled fits in both $i(\nu)$ and b-value(ν) coordinate spaces with the goodness-of-fit R^2 values >0.98 for T-Nb_2O_5 (Figure 7e,f). Having a model that is consistent with a wide range of ν conditions enables $i(\nu)$ prediction into the diffusion-limited regime. In the next section this model is used to quantitatively assess surface-limited and diffusion-limited contributions in a manner that is consistent with the expectations for simple geometric changes.

9. Example 2: Effects of Amorphization on T-Nb_2O_5 Lithiation Kinetics

As the second experimental example, the effects of amorphization upon T-Nb_2O_5 lithiation kinetics were examined with tailored nanomaterials, the same process of elimination described previously (Figure 6), and the above series model for current.[78] Amorphization, broadly defined here, is the inclusion of deliberate defects and spans a continuum of configurations between single crystals and purely disordered solids. Across a variety of intercalation-based energy storage materials, amorphization has been reported to sometimes enhance intercalation diffusion, electronic conductivity, and performance.[78,79,85,106,162–169] For example, oxygen vacancies in MoO_3 were correlated to an increase in the interlayer-spacing of its 2D crystal structure that modified its lithium diffusivity.[162] Similarly, simulations

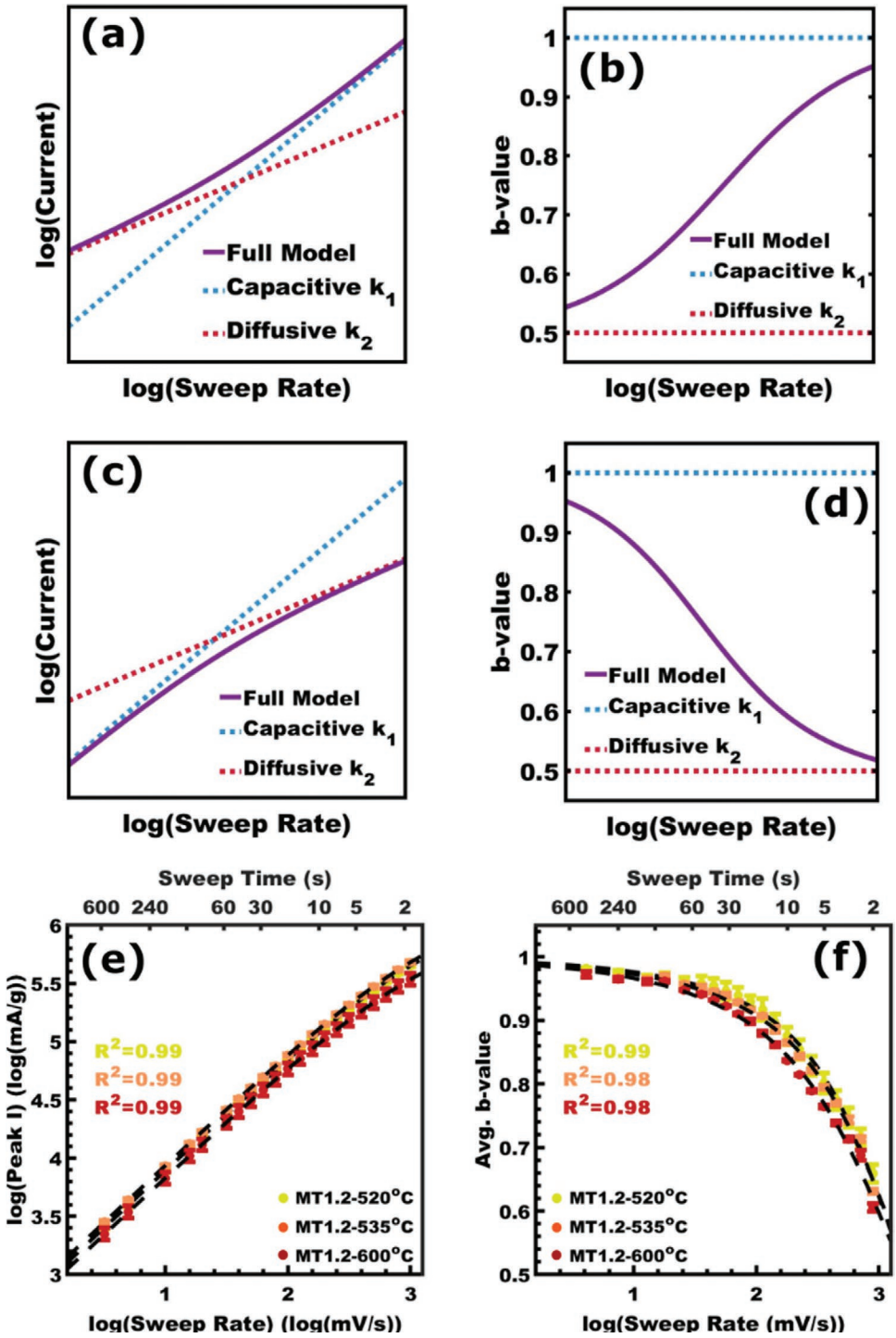

Figure 7. Comparison of a,b) (Equation (2)) parallel and c,d) (Equation (6)) series current models in $i(v)$ and b-value(v) coordinate spaces on the left and right columns, respectively. e,f) (Equation (7)) Experimental data for T-Nb_2O_5 are shown with best-fits using the series model with a third R term. Values presented as mean ± standard error-of-the-mean. Adapted with permission.[78] Copyright 2022, Wiley-VCH Verlag GmbH & Co. KGaA, Weinheim.

correlated oxygen vacancies in V_2O_5 to greater lithium diffusivity ascribed to a decreased energetic barrier to hop between intercalation sites.[170] Amorphous Nb_2O_5 was reported to have decreased capacity and slower kinetics than T-Nb_2O_5.[75] On the other hand, recent T-Nb_2O_5 reports of oxygen vacancy tuning showed improved conductivity,[85,162–164] diffusivity,[162,165] capacity,[162–166] and cycle stability[162] depending on the vacancy concentration. When comparing different nanoparticle samples there is often a challenge of ambiguity as to cause-and-effect since the heat treatments to adjust the defect chemistry often

simultaneously changes the particle size and thus the intercalation dimension. Here the use of PMT to produce tailored sets of nanomaterials can reduce this ambiguity. PMT samples were prepared over a range of M:T ratios and were calcined at temperatures between 300 and 600 °C. All of the resulting samples had a nominal pore size of ~95 nm and the wall thicknesses ranged from ~45.6-75.1 nm. The samples calcined below 520 °C were fully amorphous (non-crystalline) and were unstable to repeated (de)lithiation cycling. Relatedly a recent study identified dissolution of amorphous Nb_2O_5 content resulting from repeated cycling.[171] In contrast, the crystalline T-Nb_2O_5 samples calcined between 520–600°C were stable to cycling and exhibited markedly different lithiation kinetics depending on the calcination temperature. Here the combination of X-ray diffraction (XRD), X-ray photoelectron spectroscopy (XPS), and X-ray absorption fine structure (XAFS) identified increasing crystal growth with calcination temperature and increasing extent of crystallinity spanning from 68.4–86.4%, based on referencing a 600 °C sample as fully crystalline. Similar to the first example section, this sample series exhibited a decreasing ν_{SLT} with increasing intercalation length (increasing M:T value). Again, the combination of control experiments with changing electrolyte concentration and variation of film thickness identified that intercalation diffusion was the dominant diffusive-constraint at high ν.

Comparisons of PMT samples with the same M:T ratios (similar architectural dimensions) and different heat treatments revealed the effects of amorphization upon the lithiation kinetics. There was a monotonic increase in ν_{SLT} by ~2x with decreasing calcination temperature amongst these mostly-crystalline samples. Since the SLT depends on the balance of two processes, both a surface-limited and a diffusion-limited process, the shift in ν_{SLT} could be attributed to changes in either or both process kinetics. For example, Equations (6) and (7) indicate that an increase in the ν_{SLT} is consistent with either/both a decrease in the rate of the surface-limited process (larger k_1) or/and an increase in rate of the diffusion-limited process (smaller k_2). To distinguish between these possibilities, the series model for current was used to deconvolve these effects quantitatively. **Figure 8**a,b shows the trends for best-fit values of k_1 and k_2 for mass-normalized current data as a function of the intercalation length scale (determined by M:T ratio). Comparison of k_1 values across different calcination temperatures showed an increased impedance for the surface-limited process (slower insertion) with increasing extent of T-Nb_2O_5 amorphization (Figure 8a). Comparison of k_2 values across different calcination temperatures showed a decreased impedance for the diffusion-limited process (faster diffusion) with increasing extent of T-Nb_2O_5 amorphization (Figure 8b). Thus, the series model perspective ascribed the ν_{SLT} change from amorphization to both decelerating the surface-limited process by 17.0% and accelerating the diffusion-limited process by 12.2%. Furthermore, both k_2 comparisons with increasing wall thickness (constant calcination temperature) and $t_{SLT}^{0.5}$ were directly proportional to the intercalation length scale as expected (Figure 8b,c) for the generalized solution to Fick's second law (Equation (5)) where the increasing impedance values and increasing t_{SLT} correspond to the increasing diffusion length. Such dependencies of the pseudocapacitive response upon the intercalation length scale are not consistent with a near-surface system (Figure 3). The combination of XPS, electron paramagnetic resonance (EPR), and density functional theory (DFT) identified excess oxygen species in the amorphized samples. A range of candidate oxygen defect species were considered where the lack of a detectable EPR signal eliminated the paramagnetic candidates and suggested the presence of diamagnetic peroxide O_2^{2-}. Complimentary DFT calculations also identified the formation of such peroxide defects. Such additional Li–O interactions have previously been correlated with increased energy for lithium insertion into interstitial sites,[172] which is consistent with the k_1 trends here. These samples also exhibited remarkable rate-capability. For example, sample MT1.2-520 °C maintained 95% of its lithiation capacity (577.4 ± 17.0 C g^{-1}) with 2.25 s for delithiation (1600 C-rate equivalent), exceeding many literature precedents for T-Nb_2O_5 (Figure 8d).[51,70,75,83,92,103,173]

10. Example 3: Effects of Tailored Titania Amorphous character on Lithiation Kinetics

As the third experimental example, the effects of amorphous character upon titania lithiation kinetics were examined by combining tailored nanomaterials with the process of elimination described previously (Figure 3).[79] As compared to crystalline

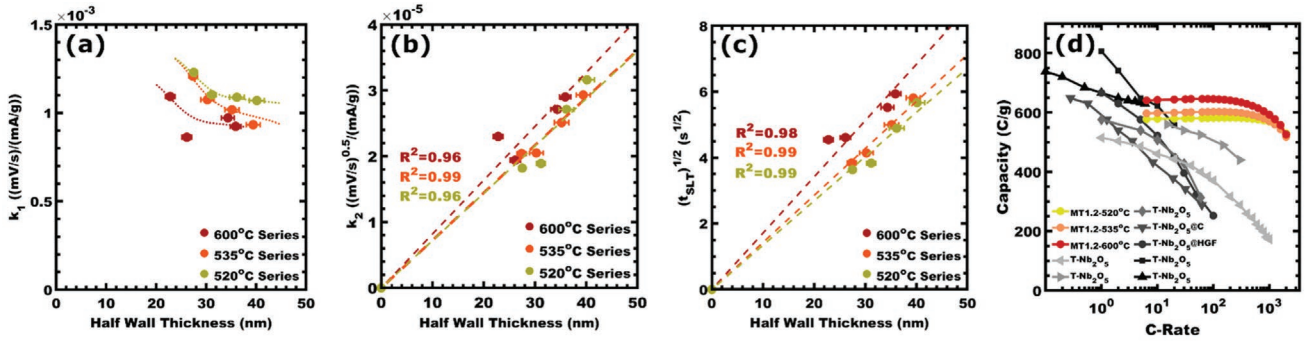

Figure 8. PMT series of T-Nb_2O_5 were calcined at different temperatures to vary the extent of amorphization prior to electrochemical analysis. CV data were fitted using Equation (7) leading to a) k_1 and b) k_2 values. c) The t_{SLT} was plotted versus the intercalation length where dashed lines correspond to fits from Equation (5) where a decreased slope indicates a greater diffusivity. d) The rate-dependent lithiation capacity for samples at 520, 535, and 600 °C were compared to literature precedents. Adapted with permission.[78] Copyright 2022, Wiley-VCH Verlag GmbH & Co. KGaA, Weinheim

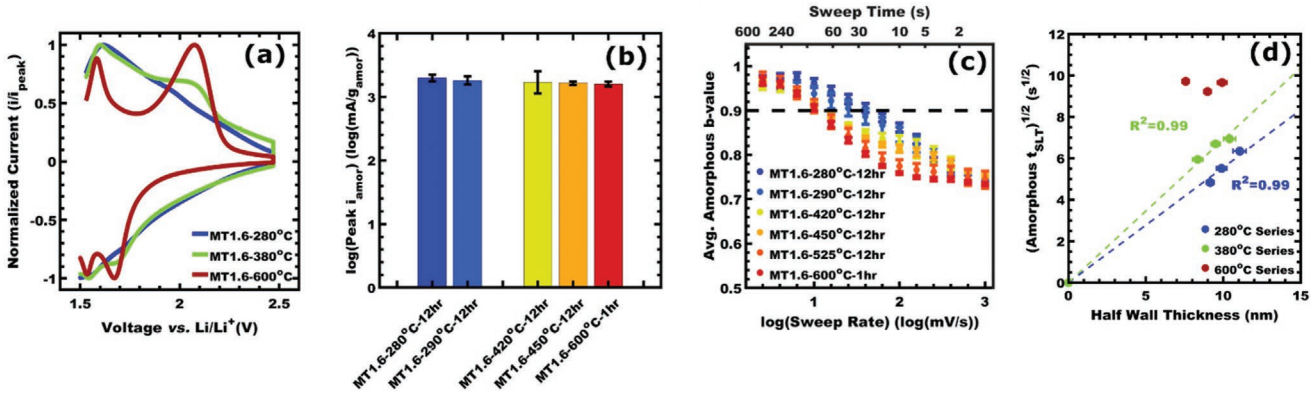

Figure 9. a) Normalized cyclic voltammograms of representative samples whose anodic peaks at ≈1.6 and ≈2.1 V were ascribed to amorphous and anatase TiO_2 phases, respectively. The amorphous phase kinetics were analyzed using the corresponding CV peaks. b) Constant $i_{amor}(v)$ were found when comparing the mass and phase normalized amorphous phase currents (2 mV s^{-1}, surface-limited regime). c) The changes in *b*-value(v) and v_{SLT} were thus attributed to changes to the intercalation rate as a result of amorphous character. d) The $t_{SLT}^{0.5}$ versus intercalation length (half wall thickness) correlated well with the direct proportionality expected from Equation (5). Values presented with error bars are the mean ± the standard error-of-the-mean. Adapted with permission.[79] Copyright 2022, Wiley-VCH Verlag GmbH & Co. KGaA, Weinheim.

anatase, amorphous TiO_2 has been shown to increase the rate of intercalation diffusion and enable pseudocapacitive current responses.[167,174,175] Similarly increased lithiation capacity and stability have been reported for metal oxides as attributed to the oxygen vacancy concentrations.[106,162–166,168,169] Whereas "perfect" crystalline materials have a well-defined arrangement of atoms, amorphous analogs of the same composition exhibit a continuum of atomic structures. Many of these atomic structures exist ephemerally during typical crystallization heat treatments. An interesting feature, however, is that nanoscale TiO_2 often stubbornly consists[47,176–179] of mixtures of polymorphs, including anatase, rutile, bronze, amorphous, and other phases. Understanding cause-and-effect with multiple phases adds the challenge of isolating the contributions of each phase. Such materials are also a unique opportunity to probe the lithiation behaviors of amorphous TiO_2 with a diversity of atomic structures. A series of PMT-derived titania architectures were prepared with ≈20 nm pore sizes and wall thicknesses ranging from ≈15–22 nm as controlled by the M:T ratio. The samples were calcined at temperatures ranging from 280—600 °C and the resulting samples were measured using CV. The presence of multiple CV peaks corresponding to different phases enabled the kinetics of each phase to be isolated whereas metrics of overall capacity would convolve all phases present (**Figure 9**a). The samples calcined at 280 and 290 °C were fully amorphous by XRD whereas those heated above 380 °C contained anatase and exhibited both phases by CV. The electrochemical kinetics were analyzed by comparison of mass normalized peak currents $i(v)$ as shown in Figure 9b. As described in prior examples, a series of architectures (calcined at 280, 380, and 600 °C) were combined with CV analysis and the process of elimination to identify intercalation as the dominant diffusive constraint for the amorphous phase in all cases. Remarkably the amorphous phase v_{SLT} increased monotonically by 317% with lowered calcination temperatures (Figure 9c). As discussed in the second example above, changes to the v_{SLT} can be caused by alteration of either the surface-limited and/or diffusion-limited processes. Predating the development of the series model (Equations (6) and (7)), disambiguation here started by comparing the peak currents at low v were to check for changes in the rate of the surface-limited process within the surface-limited v-regime. The constant peak current (normalized by phase-content) indicated that the significant changes in *b*-value(v) and v_{SLT} were associated principally with changes to the intercalation diffusion (Figure 9d). The rate-capability of samples MT1.6-280 °C compared favorably with literature precedents of high-performing TiO_2 nanomaterials.[46,167,180–182] In contrast to literature precedents[46,167,180–182] which retained lithiation capacities of ≈400 C g^{-1} ($x \approx 0.5$ in Li_xTiO_2) between C-rates of 15–80, sample MT1.6-280 °C maintained >400 C g^{-1} capacity up to an 800 C-rate (4.5 s sweep time). These results highlight how isomorphic sample series can reveal previously unidentified trends and opportunities by reducing ambiguity in multiphase samples. These marked lithiation changes with amorphous character highlight a need for new synthesis techniques and further correlations of atomic structure to lithiation behavior.

11. Relaxation Times and the Transition From battery-like Intercalation to Pseudocapacitance

We propose that intercalation pseudocapacitance (surface-limited kinetics) is a natural expectation with decreasing feature sizes due to the different power law dependencies for surface and diffusion processes. Consider a spherical particle of intercalation material with efficient external electronic and ionic contacts as modelled in detail by Zhu et. al.[39] Regardless of the relative electronic/ionic rates within the particle, the fundamental relaxation time for intercalation can be written as

$$\tau^{\delta} \propto L^2 / D_{Li}^{\delta} \tag{8}$$

where L is the particle radius (half thickness) and D is the effective chemical diffusivity for neutral lithium, including both Li^+ and e^-. The proportionality symbol accommodates various scalers including geometric parameters that would otherwise distract from the fundamental superposition of length scale and time.

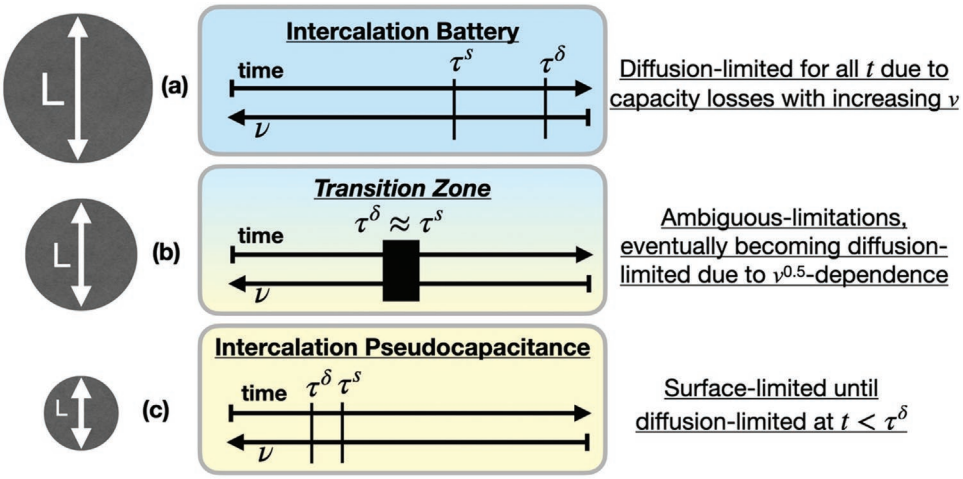

Figure 10. Surface and intercalation relaxation times scale differently with L according to Equations (8) and (9). A 2× reduction in feature size (L) is depicted where τ^δ decreases with L-reduction more quickly than τ^s, leading to behavior transitions from a) battery-like to c) capacitor-like. Time (t) and voltage sweep rate (ν) scale inversely.

When a diffusion-controlled device governed by Equation (8) is (dis)charged slowly with $t > \tau^\delta$ then the full capacity is accessible whereas faster (dis)charge times with $t < \tau^\delta$ decrease in capacity due to the ever-shallower depth of intercalation. The L^2 dependence is important to note; for example, doubling the intercalation length scale quadruples the diffusion relaxation time (i.e., 4× lower ν). Similarly, the relaxation time of the surface insertion process may be written as[39]

$$\tau^s \propto \frac{L^3}{\Gamma L^2} = L/\Gamma \tag{9}$$

where Γ is the surface reaction rate per unit area. Here L^3 is proportional to the reaction extent being stored (coulombs) and ΓL^2 is the total reaction rate (coulombs s^{-1}). The proportionality symbol again accommodates geometric parameters that were excluded to highlight the superposition of length scale and time. The τ^δ and τ^s relaxation times have different power dependencies upon length scale where Equation (8) scales with L^2 and Equation (9) scales with L^1. These different L-powers naturally lead all intercalation batteries ($\tau^\delta > \tau^s$) to transition to intercalation pseudocapacitance ($\tau^\delta < \tau^s$) with decreasing L-dimension (**Figure 10**). Though these relaxation times were previously noted individually, this is their first use to infer this transition in intercalation behaviors, to the best of our knowledge. This crossover in relaxation times where $\tau^\delta \approx \tau^s$ perhaps offers an explanation for the blurred transition between battery-like behavior and capacitor-like behavior (Figure 10b).[53,65] This crossover occurs when Equation (8) is equal to Equation (9). Assuming all proportionality constants equal one leads to

$$1 = \frac{L\Gamma}{D_{\mathrm{Li}}^\delta} \tag{10}$$

It is apparent that all ratios of $\Gamma/D_{\mathrm{Li}}^\delta$ have a corresponding L-value satisfying Equation (10). Thus, this relationship predicts that all intercalation materials are expected to transition their behavior from diffusion-limited to surface-limited at a critical value of L. This is consistent with numerous observations of battery materials transitioning to surface-limited pseudocapacitive kinetics with nanoscale dimensions. Furthermore, Equations (8) and (10) appear incompatible with the notion of intrinsic intercalation pseudocapacitance, again since all materials are expected to exhibit a transition in behavior at a critical L-value. Please note that intercalation batteries are not expected to transition to surface-limited kinetics with increasing ν (decreasing t) since the $t^{0.5}$ intercalation dependence decreases capacity, effectively continuously shifting τ^s to smaller values. Furthermore, the same scaling laws predict that intercalation pseudocapacitive electrodes transition to diffusion-limited behavior when $t < \tau^\delta$. This expectation (Figure 9c) is consistent with the three experimental examples elaborated above in sections and the concept of Insert-Intercalate systems (Figure 3).

12. Connecting the Series-Model to Performance Outlooks

The above examples have showed how both the insertion reaction rate and the intercalation rate affect performance. Whereas intercalation pseudocapacitive electrodes are generally used in the surface-limited ν-regime (for definition sake) there is also much interest in applying similar fast intercalation materials in the diffusion-limited regime for the sake of increased energy density.[38] The superposition of architecture dimensions, timescale, and rate coefficients was elegantly described recently using three governing unitless parameter (l, γ, Λ).[153] The two divergent use cases above benefit from improvements to different processes. For example, pseudocapacitive electrodes operated in the surface-limited regime would naturally be improved by accelerating the surface-limited process. **Figure 11** compares $i(\nu)$ calculated using Equation (6) using the best-fit values for a T-Nb_2O_5 sample with MT = 1.2 calcined at 535 °C (k_1 = norm) to predicted results with hypothetical progressive decreases in the k_1 surface impedance (faster surface reaction). For example, if focused on $\nu = 100$ mV s^{-1} (200 C-rate equivalent) would result

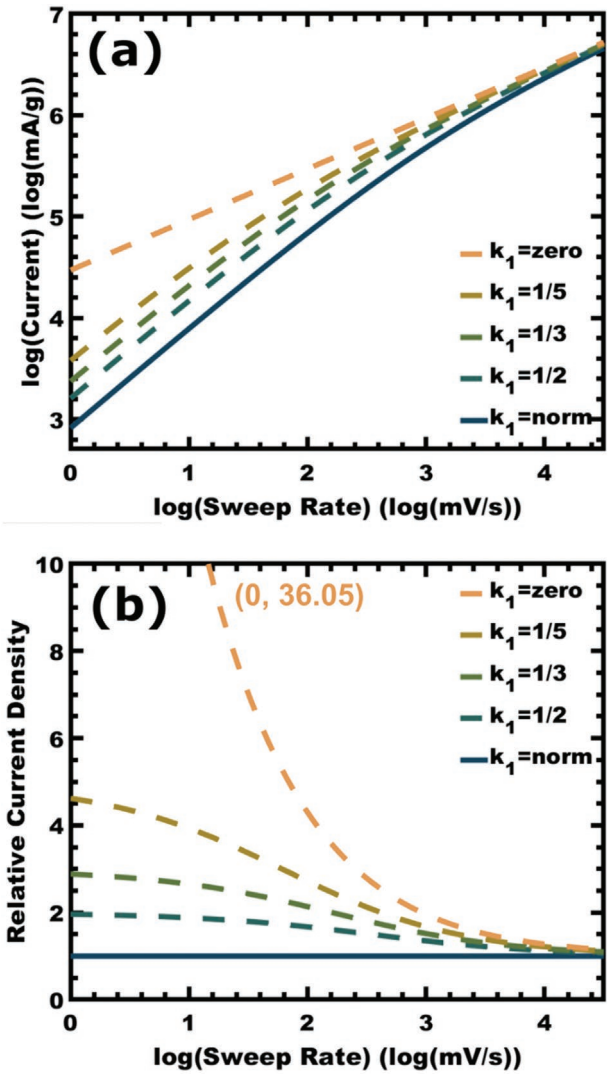

Figure 11. a) Hypothetical plots based on Equation (6) starting from best-fits for a T-Nb_2O_5 MT = 1.2, 535 °C sample ("norm") and step-wise reducing the impedance of the surface limited process to zero (k_1 value). a) The log–log plots of $i(\nu)$ are shown for a range of hypothetical conditions and b) the corresponding relative current densities are also shown.

in a 67% increase in relative current with a 50% reduction in k_1. The reduction of k_1 to zero represents a rationale model limit correspond to a purely diffusion-limited device where the relative current predicted at $\nu = 100$ mV s^{-1} could increase by 434%. On the other hand, increasing the diffusion rate would enable the ν_{SLT} to move to higher ν. As pointed out recently, consumers are probably not interested in the mechanism or rate limiting step so much as actual performance[55] so mechanism transition points are a questionable performance target. In contrast, the pursuit of rapid (dis)charging designs maintaining battery-like energy densities at the device level should principally focus on improvements to transport processes, mainly the intercalation diffusivity but also the electrical conductivity.[38] Practitioners in the energy storage field continue to make rapid improvements to materials and device capabilities. There is not yet a clear limit for the future capabilities of rapid intercalation materials.

13. Future Directions for Synthesis and Characterization

Several promising future directions are suggested including electrochemical characterizations and synthetic capabilities. The above three experimental example sections using tailored nanomaterials correlated simplistic descriptors to changes in specific transport processes. The desire there to minimize assumptions, however, reduces the number of fitted values and thus also limits the number of insights. There is room to apply more detailed electrochemical analyses while still minimizing assumptions. For examples EIS is itself a measurement technique without inherent models or assumptions until the data is interpreted. The limitations of equivalent circuit analysis were discussed, vide supra. So called 3D Bode analysis[81,126,183,184] is a route to interpret EIS data without the hazards of equivalent circuits. In the context of intercalation materials, this technique examines the real C' and imaginary C″ capacitances as derived from impedance magnitudes and phase angles. 3D Bode analysis can distinguish fast, reversible (surface-limited) and slower, irreversible (diffusion-limited) dissipative processes as a function of voltage and frequency. Additionally, this technique can provide time constants for behavior transitions. Combining 3D bode analysis with tailored nanomaterials and the process of elimination could deepen the understanding of intercalation pseudocapacitance. One advantage of the EIS techniques over CV is that ohmic shifts are avoided by using small voltage fluctuations upon a steady state average voltage. In the opposite vein, comprehensive models[59,77,82,116,125,127,153–156] attempting to capture all possible processes present a different challenge where the number of parameters can become overwhelming with the following variable categories: transfer processes, ion/electron transport, and concentration gradients within all phases, interaction coefficients, material capacitance, material geometry, and overpotential. Ideally those parameters could be fitted with numerous measurements from a closely related set of samples to avoid collecting mismatched values from disparate literature reports and varying synthetic methods. There is opportunity for comprehensive models to reveal much more mechanistic detail, however the tractability of collecting dozens of accurate experimental measures remains a challenge. There appears to be room for faster progress in the short term based on using simpler models if disambiguation can be managed. There is also room for intermittent titration techniques (ITT) to contribute to the understanding of fast intercalation materials.[185,186] ITT methods take discrete steps in voltage or current that allow for subsequent decay in current or voltage, respectively. The models for ITT however assume purely diffusion-limited kinetics where adaptations of these models could benefit the understanding of intercalation pseudocapacitance.[185,186] Regardless of the analytical technique, there is a need to include control experiments that, for example, reduce the ambiguity of concomitant diffusive processes and ideally also integrate series of architectures to cleanly interrogate the effects of changing the intercalation dimension independently.

Synthetic opportunities for improvements exist at both the surface and the bulk locations. The surface-limited faradaic process can be altered both by the defect chemistry[78,79,85,106,162–169] as well as by surface coatings.[187–194] For example a recent paper

reported nitridation coating of $FeNb_{11}O_{29}$ that reduced the charge transfer resistance of the insertion process by improving the desolvation process and preventing solvent cointercalation.[195] Recent DFT calculations suggest that the desolvation process may be the rate limiting sub-step during the surface faradaic insertion reaction.[196] Bulk crystalline inorganic material properties are also quickly advancing with, for example, the recent development of range of Wadsley–Roth niobates, many of which exhibit rapid intercalation.[38,40,197] For a number of these phases, the niobium oxidation state ranges from 5+ to 3+ during cycling, exceeding the typical capacity limit associated with just one lithium atom per metal atom. The inclusion of rapid lithium transport with low hopping barriers and a lack of first order phase transitions is important to enable high intercalation rates. The ability to tailor these and other emerging crystalline materials with defect engineering or amorphization has shown recent promise.[40] It is our opinion that amorphous phases are quite underexplored in part due to the tremendous diversity of amorphous and amorphized atomic configurations. As highlighted in the third example above, amorphous TiO_2 can change its lithiation behavior markedly depending on its processing history. New synthesis methodologies that span this continuum of atomic configurations between pure disorder and classical crystalline order are a promising future direction. There are significant synthetic opportunities to advance all facets of rapid intercalation materials, from amorphous to crystalline and from the interior to the surface.

14. Conclusion

The demand for rapid (dis)charging energy storage has motivated much research with nanoscale materials. Beyond accelerated kinetics owing to reduced feature sizes, nanomaterials were shown early on to enable changes to the reaction path thermodynamics, intercalant solubility, and reversibility. The investigation of rapid (dis)charging intercalation nanomaterials led to the discovery of intercalation pseudocapacitance with surface-limited $i(v)$. The high-power performance of pseudocapacitive devices generated much excitement while at the same time initiating much dialog about their operating mechanisms. For example, Figure 3 presented two perspectives for charge storage in intercalation pseudocapacitive electrodes (Insert-Intercalate or Near-Surface) and Figure 7 presented the corresponding $i(v)$ models. This review highlights how systematic nanoscale synthesis procedures such as persistent micelle templates can reveal new insights to such emergent electrochemical phenomena. Specifically, we advocate for the combination of tailored nanomaterials with a process of elimination strategy to isolate the effect of each transport process upon electrochemical kinetics. This strategy aids the disambiguation of multiple diffusive processes, all of which follow the same scaling laws with time. Three example studies were described with multiple intercalation pseudocapacitive materials where the timescales exhibiting surface-limited kinetics depended on the total intercalation length scale. A recent series model for current was described which accurately matches experimental data for $i(v)$ and b-value(v) across wide spanning timescales from the Insert-Intercalate perspective. An example showed how the series model can isolate material-specific $i(v)$ effects such as how amorphization modifies both the insertion and diffusion kinetics. The collection of examples and data assembled here were most consistent with the Insert-Intercalate perspective and were inconsistent with the Near-Surface perspective. Looking toward enhancing capabilities, avenues for both faster intercalation pseudocapacitance and increased energy density were discussed from the perspective of the series model for current. A new argument based on relaxation times was suggested to explain the continuum between battery-like and pseudocapacitive behaviors upon nanoscaling the feature sizes. The presented scaling laws for intercalation relaxation times in addition to volumes of experimental evidence suggest that the notion of intrinsic intercalation pseudocapacitance is not supported. Future directions were suggested including analytical methods that minimize assumptions such as 3D Bode in addition to new synthetic methods that emphasize the expansive continuum between amorphous and crystalline materials as well as tailored defects and coatings.

Acknowledgements

W.v.d.B. and M.S. acknowledge support by the NSF CAREER program, NSF Award No. DMR-1752615. The authors thank Sean Wechsler for proofreading the manuscript.

Conflict of Interest

The authors declare no conflict of interest.

Keywords

battery, intercalation, kinetics, nanomaterials, pseudocapacitance

Received: April 12, 2022
Revised: May 12, 2022
Published online: June 1, 2022

[1] J. H. Lee, S. J. Hardman, G. Tal, *Energy Res. Soc. Sci.* **2019**, *55*, 218.
[2] G. Berckmans, M. Messagie, J. Smekens, N. Omar, L. Vanhaverbeke, J. Van Mierlo, *Energies* **2017**, *10*, 1314.
[3] National Blueprint for Lithium Batteries 2021–2030, Department of Energy, **2021**, p. 24.
[4] G. Ewing, E. Sarigöllü, *J. Public Policy Mark.* **2018**, *19*.
[5] B. Lane, S. Potter, *J. Clean. Prod.* **2007**, *15*, 1085.
[6] S.-K. Jung, I. Hwang, D. Chang, K.-Y. Park, S. J. Kim, W. M. Seong, D. Eum, J. Park, B. Kim, J. Kim, J. H. Heo, K. Kang, *Chem. Rev.* **2020**, *120*, 6684.
[7] Y. Choi, S. Pyun, *Solid State Ion.* **1997**, *99*, 173.
[8] M. Okubo, E. Hosono, J. Kim, M. Enomoto, N. Kojima, T. Kudo, H. Zhou, I. Honma, *J. Am. Chem. Soc.* **2007**, *129*, 7444.
[9] A. K. Stephan, *Joule* **2019**, *3*, 2583.
[10] M. Wagemaker, R. van de Krol, A. P. M. Kentgens, A. A. van Well, F. M. Mulder, *J. Am. Chem. Soc.* **2001**, *123*, 11454.
[11] M. Wagemaker, W. J. H. Borghols, F. M. Mulder, *J. Am. Chem. Soc.* **2007**, *129*, 4323.

[12] M. Wagemaker, G. J. Kearley, A. A. van Well, H. Mutka, F. M. Mulder, *J. Am. Chem. Soc.* **2003**, *125*, 840.
[13] A. Yamada, H. Koizumi, S. Nishimura, N. Sonoyama, R. Kanno, M. Yonemura, T. Nakamura, Y. Kobayashi, *Nat. Mater.* **2006**, *5*, 357.
[14] N. Meethong, H.-Y. S. Huang, W. C. Carter, Y.-M. Chiang, *Electrochem. Solid-State Lett.* **2007**, *10*, A134.
[15] G. Kobayashi, S. Nishimura, M.-S. Park, R. Kanno, M. Yashima, T. Ida, A. Yamada, *Adv. Funct. Mater.* **2009**, *19*, 395.
[16] M. Wagemaker, D. P. Singh, W. J. H. Borghols, U. Lafont, L. Haverkate, V. K. Peterson, F. M. Mulder, *J. Am. Chem. Soc.* **2011**, *133*, 10222.
[17] G. Chen, X. Song, T. J. Richardson, *Electrochem. Solid-State Lett.* **2006**, *9*, A295.
[18] W. J. H. Borghols, M. Wagemaker, U. Lafont, E. M. Kelder, F. M. Mulder, *J. Am. Chem. Soc.* **2009**, *131*, 17786.
[19] L. Kavan, J. Procházka, T. M. Spitler, M. Kalbáč, M. Zukalová, T. Drezen, M. Grätzel, *J. Electrochem. Soc.* **2003**, *150*, A1000.
[20] M. Wagemaker, F. M. Mulder, A. Van der Ven, *Adv. Mater.* **2009**, *21*, 2703.
[21] H. Wang, Y.-I. Jang, B. Huang, D. R. Sadoway, Y.-M. Chiang, *J. Electrochem. Soc.* **1999**, *146*, 473.
[22] M. T. McDowell, S. W. Lee, W. D. Nix, Y. Cui, *Adv. Mater.* **2013**, *25*, 4966.
[23] S. W. Lee, M. T. McDowell, J. W. Choi, Y. Cui, *Nano Lett.* **2011**, *11*, 3034.
[24] Y. Yao, M. T. McDowell, I. Ryu, H. Wu, N. Liu, L. Hu, W. D. Nix, Y. Cui, *Nano Lett.* **2011**, *11*, 2949.
[25] J. Li, K. He, Q. Meng, X. Li, Y. Zhu, S. Hwang, K. Sun, H. Gan, Y. Zhu, Y. Mo, E. A. Stach, D. Su, *ACS Nano* **2016**, *10*, 9577.
[26] Y. Fu, X. Guo, Z. Xu, G. Zhao, C. Xu, Y. Zhu, L. Zhou, *ACS Appl. Mater. Interfaces* **2021**, *13*, 28171.
[27] H. Huang, S.-C. Yin, L. F. Nazar, *Electrochem. Solid-State Lett.* **2001**, *4*, A170.
[28] K. Kanamura, K. Shiraishi, K. Dokko, *Phosphorus Res. Bull.* **2005**, *19*, 152.
[29] R. Malik, D. Burch, M. Bazant, G. Ceder, *Nano Lett.* **2010**, *10*, 4123.
[30] J. Christensen, J. Newman, *J. Electrochem. Soc.* **2006**, *153*, A1019.
[31] W. E. Gent, Y. Li, S. Ahn, J. Lim, Y. Liu, A. M. Wise, C. B. Gopal, D. N. Mueller, R. Davis, J. N. Weker, J.-H. Park, S.-K. Doo, W. C. Chueh, *Adv. Mater.* **2016**, *28*, 6631.
[32] P. P. R. M. L. Harks, F. M. Mulder, P. H. L. Notten, *J. Power Sources* **2015**, *288*, 92.
[33] Q. Xiao, M. Gu, H. Yang, B. Li, C. Zhang, Y. Liu, F. Liu, F. Dai, L. Yang, Z. Liu, X. Xiao, G. Liu, P. Zhao, S. Zhang, C. Wang, Y. Lu, M. Cai, *Nat. Commun.* **2015**, *6*, 8844.
[34] S. H. Lee, S.-H. Yu, J. E. Lee, A. Jin, D. J. Lee, N. Lee, H. Jo, K. Shin, T.-Y. Ahn, Y.-W. Kim, H. Choe, Y.-E. Sung, T. Hyeon, *Nano Lett.* **2013**, *13*, 4249.
[35] S. Payandeh, D. Goonetilleke, M. Bianchini, J. Janek, T. Brezesinski, *Curr. Opin. Electrochem.* **2022**, *31*, 100877.
[36] Y.-T. Cheng, M. W. Verbrugge, *J. Appl. Phys.* **2008**, *104*, 083521.
[37] X. Zhang, W. Shyy, A. M. Sastry, *J. Electrochem. Soc.* **2007**, *154*, A910.
[38] K. J. Griffith, K. M. Wiaderek, G. Cibin, L. E. Marbella, C. P. Grey, *Nature* **2018**, *559*, 556.
[39] C. Zhu, R. E. Usiskin, Y. Yu, J. Maier, *Science* **2017**, *15*, 358.
[40] Y. Yang, J. Zhao, *Adv. Sci.* **2021**, *8*, 2004855.
[41] B. E. Conway, E. Gileadi, *Trans. Faraday Soc* **1962**, *58*, 2493.
[42] H. Lindström, S. Södergren, A. Solbrand, H. Rensmo, J. Hjelm, A. Hagfeldt, S.-E. Lindquist, *J. Phys. Chem. B* **1997**, *101*, 7717.
[43] S. Trasatti, G. Buzzanca, *J. Electroanal. Chem. Interf. Electrochem.* **1971**, *29*, A1.
[44] J. P. Zheng, P. J. Cygan, T. R. Jow, *J. Electrochem. Soc.* **1995**, *142*, 2699.
[45] H. Y. Lee, J. B. Goodenough, *J. Solid State Chem.* **1999**, *144*, 220.
[46] A. R. Armstrong, G. Armstrong, J. Canales, R. García, P. G. Bruce, *Adv. Mater.* **2005**, *17*, 862.
[47] M. Zukalová, M. Kalbáč, L. Kavan, I. Exnar, M. Graetzel, *Chem. Mater.* **2005**, *17*, 1248.
[48] W. Dong, D. R. Rolison, B. Dunna, *Electrochem. Solid-State Lett.* **2000**, *3*, 457.
[49] T. Brezesinski, J. Wang, S. H. Tolbert, B. Dunn, *Nat. Mater.* **2010**, *9*, 146.
[50] K. Brezesinski, J. Wang, J. Haetge, C. Reitz, S. O. Steinmueller, S. H. Tolbert, B. M. Smarsly, B. Dunn, T. Brezesinski, *J. Am. Chem. Soc.* **2010**, *132*, 6982.
[51] V. Augustyn, J. Come, M. A. Lowe, J. W. Kim, P.-L. Taberna, S. H. Tolbert, H. D. Abruña, P. Simon, B. Dunn, *Nat. Mater.* **2013**, *12*, 518.
[52] C. Choi, D. S. Ashby, D. M. Butts, R. H. DeBlock, Q. Wei, J. Lau, B. Dunn, *Nat. Rev. Mater.* **2020**, *5*, 5.
[53] Y. Gogotsi, R. M. Penner, *ACS Nano* **2018**, *12*, 2081.
[54] Y. Liu, S. P. Jiang, Z. Shao, *Mater. Today* **2020**, *7*, 100072.
[55] S. Fleischmann, J. B. Mitchell, R. Wang, C. Zhan, D. Jiang, V. Presser, V. Augustyn, *Chem. Rev.* **2020**, *120*, 6738.
[56] A. Eftekhari, M. Mohamedi, *Mater. Today Energy* **2017**, *6*, 211.
[57] V. Augustyn, P. Simon, B. Dunn, *Energy Environ. Sci.* **2014**, *7*, 1597.
[58] T. Brousse, D. Bélanger, J. W. Long, *J. Electrochem. Soc.* **2015**, *162*, A5185.
[59] C. Costentin, T. R. Porter, J.-M. Savéant, *ACS Appl. Mater. Interfaces* **2017**, *9*, 8649.
[60] C. Costentin, J.-M. Savéant, *Chem. Sci.* **2019**, *10*, 5656.
[61] Z. Gan, J. Yin, X. Xu, Y. Cheng, T. Yu, *ACS Nano* **2022**, *61*, 5131.
[62] S. Fleischmann, Y. Zhang, X. Wang, P. T. Cummings, J. Wu, P. Simon, Y. Gogotsi, V. Presser, V. Augustyn, *Nat. Energy* **2022**, *7*, 222.
[63] C. Costentin, *J. Phys. Chem. Lett.* **2020**, *11*, 9846.
[64] W. Dmowski, T. Egami, K. E. Swider-Lyons, C. T. Love, D. R. Rolison, *J. Phys. Chem. B* **2002**, *106*, 12677.
[65] P. Simon, Y. Gogotsi, B. Dunn, *Science* **2014**, *343*, 1210.
[66] G. Z. Chen, *Int. Mater. Rev.* **2017**, *62*, 173.
[67] J. Come, V. Augustyn, J. W. Kim, P. Rozier, P.-L. Taberna, P. Gogotsi, J. W. Long, B. Dunn, P. Simon, *J. Electrochem. Soc.* **2014**, *161*, A718.
[68] J. B. Cook, H.-S. Kim, Y. Yan, J. S. Ko, S. Robbennolt, B. Dunn, S. H. Tolbert, *Adv. Energy Mater.* **2016**, *6*, 1501937.
[69] B. Reichman, A. J. Bard, *J. Electrochem. Soc.* **1981**, *128*, 344.
[70] K. J. Griffith, A. C. Forse, J. M. Griffin, C. P. Grey, *J. Am. Chem. Soc.* **2016**, *138*, 8888.
[71] S. Li, Q. Xu, E. Uchaker, X. Cao, G. Cao, *CrystEngComm* **2016**, *18*, 2532.
[72] X. Qu, Y. Liu, B. Li, B. Xing, G. Huang, C. Zhang, S. W. Hong, J. Yu, Y. Cao, *Energy Fuels* **2020**, *34*, 3887.
[73] D. P. Opra, S. V. Gnedenkov, S. L. Sinebryukhov, *J. Power Sources* **2019**, *442*, 227225.
[74] V. Etacheri, Y. Kuo, A. V. der Ven, B. M. Bartlett, *J. Mater. Chem. A* **2013**, *1*, 12028.
[75] J. W. Kim, V. Augustyn, B. Dunn, *Adv. Energy Mater.* **2012**, *2*, 141.
[76] T.-C. Liu, W. G. Pell, B. E. Conway, S. L. Roberson, *J. Electrochem. Soc.* **1998**, *145*, 1882.
[77] M. Forghani, S. W. Donne, *J. Electrochem. Soc.* **2019**, *166*, A1370.
[78] W. van den Bergh, S. Wechsler, H. N. Lokupitiya, L. Jarocha, K. Kim, J. Chapman, K. E. Kweon, B. C. Wood, S. Heald, M. Stefik, *Batteries Supercaps* **2022**, https://doi.org/10.1002/batt.202200056.
[79] W. van den Bergh, T. Larison, M. Stefik, *Batteries Supercaps* **2022**, https://doi.org/10.1002/batt.202200122.
[80] W. van den Bergh, H. N. Lokupitiya, N. A. Vest, B. Reid, S. Guldin, M. Stefik, *Adv. Funct. Mater.* **2021**, *31*, 2007826.
[81] J. S. Ko, C.-H. Lai, J. W. Long, D. R. Rolison, B. Dunn, J. Nelson Weker, *ACS Appl. Mater. Interfaces* **2020**, *12*, 14071.

[82] H.-L. Girard, B. Dunn, L. Pilon, *Electrochim. Acta* **2016**, *211*, 420.
[83] E. Lim, C. Jo, H. Kim, M.-H. Kim, Y. Mun, J. Chun, Y. Ye, J. Hwang, K.-S. Ha, K. C. Roh, K. Kang, S. Yoon, J. Lee, *ACS Nano* **2015**, *9*, 7497.
[84] X. Ge, C. Gu, Z. Yao, J. Sun, X. Wang, J. Tu, *Chem. Eng. J.* **2018**, *338*, 211.
[85] L. Kong, X. Liu, J. Wei, S. Wang, B. B. Xu, D. Long, F. Chen, *Nanoscale* **2018**, *10*, 14165.
[86] W. Luo, Y. Li, J. Dong, J. Wei, J. Xu, Y. Deng, D. Zhao, *Agnew. Chem.* **2013**, *125*, 10699.
[87] Y. Lian, D. Wang, S. Hou, C. Ban, J. Zhao, H. Zhang, *Electrochim. Acta* **2020**, *330*, 135204.
[88] S. Hemmati, G. Li, X. Wang, Y. Ding, Y. Pei, A. Yu, Z. Chen, *Nano Energy* **2019**, *56*, 118.
[89] G. Luo, H. Li, D. Zhang, L. Gao, T. Lin, *Electrochim. Acta* **2017**, *235*, 175.
[90] J. Y. Cheong, J.-W. Jung, D.-Y. Youn, C. Kim, S. Yu, S.-H. Cho, K. R. Yoon, I.-D. Kim, *J. Power Sources* **2017**, *360*, 434.
[91] C. Shi, K. Xiang, Y. Zhu, W. Zhou, X. Chen, H. Chen, *Ceram. Int.* **2017**, *43*, 12388.
[92] B. Deng, T. Lei, W. Zhu, L. Xiao, J. Liu, *Adv. Funct. Mater.* **2018**, *28*, 1704330.
[93] H. Yang, H. Xu, L. Wang, L. Zhang, Y. Huang, X. Hu, *Chem. – Eur. J.* **2017**, *23*, 4203.
[94] H. Song, J. Fu, K. Ding, C. Huang, K. Wu, X. Zhang, B. Gao, K. Huo, X. Peng, P. K. Chu, *J. Power Sources* **2016**, *328*, 599.
[95] S. Lou, X. Cheng, L. Wang, J. Gao, Q. Li, Y. Ma, Y. Gao, P. Zuo, C. Du, G. Yin, *J. Power Sources* **2017**, *361*, 80.
[96] D. Li, J. Shi, H. Liu, C. Liu, G. Dong, H. Zhang, Y. Yang, G. Lu, H. Wang, *Sustainable Energy Fuels* **2019**, *3*, 1055.
[97] E. Lim, C. Jo, M. S. Kim, M.-H. Kim, J. Chun, H. Kim, J. Park, K. C. Roh, K. Kang, S. Yoon, J. Lee, *Adv. Funct. Mater.* **2016**, *26*, 3711.
[98] P. Nagaraju, R. Vasudevan, A. Alsalme, A. Alghamdi, M. Arivanandhan, R. Jayavel, *Nanomaterials* **2020**, *10*, 160.
[99] M. Y. Song, N. R. Kim, H. J. Yoon, S. Y. Cho, H.-J. Jin, Y. S. Yun, *ACS Appl. Mater. Interfaces* **2017**, *9*, 2267.
[100] L. Kong, C. Zhang, S. Zhang, J. Wang, R. Cai, C. Lv, W. Qiao, L. Ling, D. Long, *J. Mater. Chem. A* **2014**, *2*, 17962.
[101] G. Ma, K. Li, Y. Li, B. Gao, T. Ding, Q. Zhong, J. Su, L. Gong, J. Chen, L. Yuan, B. Hu, J. Zhou, K. Huo, *ChemElectroChem* **2016**, *3*, 1360.
[102] W. Hu, S. Zhang, W. Zhang, M. Wang, F. Feng, *J. Nanopart. Res.* **2020**, *22*, 57.
[103] H. Sun, L. Mei, J. Liang, Z. Zhao, C. Lee, H. Fei, M. Ding, J. Lau, M. Li, C. Wang, X. Xu, G. Hao, B. Papandrea, I. Shakir, B. Dunn, Y. Huang, X. Duan, *Science* **2017**, *356*, 599.
[104] S. Kim, J. Hwang, J. Lee, J. Lee, *Sci. Adv.* **2020**, *6*, eabb3814.
[105] F. Idrees, J. Hou, C. Cao, F. K. Butt, I. Shakir, M. Tahir, F. Idrees, *Electrochim. Acta* **2016**, *216*, 332.
[106] Z. Chen, H. Li, X. Lu, L. Wu, J. Jiang, S. Jiang, J. Wang, H. Dou, X. Zhang, *ChemElectroChem* **2018**, *5*, 1516.
[107] J. Zhai, Y. Wu, X. Zhao, Q. Yang, *J. Alloys Compd.* **2017**, *715*, 275.
[108] J. W. Kim, S.-O. Kim, H.-S. Kim, *Int. J. Energy Res.* **2019**, *43*, 4359.
[109] J. Hu, J. Li, K. Wang, H. Xia, *Electrochim. Acta* **2020**, *331*, 135364.
[110] X. Xu, B. Tian, S. Zhang, J. Kong, D. Zhao, B. Liu, *Anal. Chim. Acta* **2004**, *519*, 31.
[111] E. Lim, H. Kim, C. Jo, J. Chun, K. Ku, S. Kim, H. I. Lee, I.-S. Nam, S. Yoon, K. Kang, J. Lee, *ACS Nano* **2014**, *8*, 8968.
[112] A. L. Viet, M. V. Reddy, R. Jose, B. V. R. Chowdari, S. Ramakrishna, *J. Phys. Chem. C* **2010**, *114*, 664.
[113] S. Ouendi, C. Arico, F. Blanchard, J.-L. Codron, X. Wallart, P. L. Taberna, P. Roussel, L. Clavier, P. Simon, C. Lethien, *Energy Storage Mater.* **2019**, *16*, 581.
[114] S. Zhang, J. Wu, J. Wang, W. Qiao, D. Long, L. Ling, *J. Power Sources* **2018**, *396*, 88.
[115] Y.-Y. Won, D. Ramkrishna, *ACS Omega* **2019**, *4*, 11215.
[116] B.-A. Mei, J. Lau, T. Lin, S. H. Tolbert, B. S. Dunn, L. Pilon, *J. Phys. Chem. C* **2018**, *122*, 24499.
[117] B. E. Conway, W. G. Pell, *J. Power Sources* **2002**, *105*, 169.
[118] O. Bohlen, J. Kowal, D. U. Sauer, *J. Power Sources* **2007**, *172*, 468.
[119] S. Yoon, C. W. Lee, S. M. Oh, *J. Power Sources* **2010**, *195*, 4391.
[120] M. Kaus, J. Kowal, D. U. Sauer, *Electrochim. Acta* **2010**, *55*, 7516.
[121] R. L. Spyker, R. M. Nelms, *IEEE Trans. Aerosp. Electron. Syst.* **2000**, *36*, 829.
[122] M. Z. Bazant, K. Thornton, A. Ajdari, *Phys. Rev. E* **2004**, *70*, 021506.
[123] K. T. Chu, M. Z. Bazant, *Phys. Rev. E* **2006**, *74*, 011501.
[124] L. Højgaard Olesen, M. Z. Bazant, H. Bruus, *Phys. Rev. E* **2010**, *82*, 011501.
[125] B.-A. Mei, O. Munteshari, J. Lau, B. Dunn, L. Pilon, *J. Phys. Chem. C* **2018**, *122*, 194.
[126] J. S. Ko, M. B. Sassin, D. R. Rolison, J. W. Long, *Electrochim. Acta* **2018**, *275*, 225.
[127] B.-A. Mei, L. Pilon, *Electrochim. Acta* **2017**, *255*, 168.
[128] H. N. Lokupitiya, A. Jones, B. Reid, S. Guldin, M. Stefik, *Chem. Mater.* **2016**, *28*, 1653.
[129] K. A. Lantz, N. B. Clamp, W. van den Bergh, A. Sarkar, M. Stefik, *Small* **2019**, *15*, 1900393.
[130] A. Sarkar, A. Thyagarajan, A. Cole, M. Stefik, *Soft Matter* **2019**, *15*, 5193.
[131] A. Sarkar, L. Evans, M. Stefik, *Langmuir* **2018**, *34*, 5738.
[132] Y. Ma, T. P. Lodge, *Macromolecules* **2016**, *49*, 9542.
[133] S.-H. Choi, T. P. Lodge, F. S. Bates, *Phys. Rev. Lett.* **2010**, *104*, 047802.
[134] T. Larison, M. Stefik, *Langmuir* **2021**, *37*, 9817.
[135] E. R. Williams, P. L. McMahon, J. E. Reynolds, J. L. Snider, V. Stavila, M. D. Allendorf, M. Stefik, *Mater. Adv.* **2021**, *2*, 5381.
[136] M. Stefik, *J. Mater. Res.* **2021**.
[137] L. Shen, Z. Chen, *Chem. Eng. Sci.* **2007**, *62*, 3748.
[138] A. Vu, Y. Qian, A. Stein, *Adv. Energy Mater.* **2012**, *2*, 1056.
[139] P. Sutton, P. Bennington, S. N. Patel, M. Stefik, U. B. Wiesner, P. F. Nealey, U. Steiner, I. Gunkel, *Adv. Funct. Mater.* **2019**, *29*, 1905977.
[140] R. Dehmel, J. A. Dolan, Y. Gu, U. Wiesner, T. D. Wilkinson, J. J. Baumberg, U. Steiner, B. D. Wilts, I. Gunkel, *Macromolecules* **2017**, *50*, 6255.
[141] P. Docampo, S. Guldin, M. Stefik, P. Tiwana, M. C. Orilall, S. Hüttner, H. Sai, U. Wiesner, U. Steiner, H. J. Snaith, *Adv. Funct. Mater.* **2010**, *20*, 1787.
[142] E. J. W. Crossland, M. Nedelcu, C. Ducati, S. Ludwigs, M. A. Hillmyer, U. Steiner, H. J. Snaith, *Nano Lett.* **2009**, *9*, 2813.
[143] E. J. W. Crossland, P. Cunha, S. Ludwigs, M. A. Hillmyer, U. Steiner, *ACS Appl. Mater. Interfaces* **2011**, *3*, 1375.
[144] M. Nedelcu, J. Lee, E. J. W. Crossland, S. C. Warren, M. C. Orilall, S. Guldin, S. Hüttner, C. Ducati, D. Eder, U. Wiesner, U. Steiner, H. J. Snaith, *Soft Matter* **2008**, *5*, 134.
[145] A. Sarkar, M. Stefik, *J. Mater. Chem. A* **2017**, *5*, 11840.
[146] W. van den Bergh, E. R. Williams, N. A. Vest, P.-H. Chiang, M. Stefik, *Langmuir* **2021**, *37*, 12874.
[147] T. Marks, S. Trussler, A. J. Smith, D. Xiong, J. R. Dahn, *J. Electrochem. Soc.* **2011**, *158*, A51.
[148] V. Murray, D. S. Hall, J. R. Dahn, *J. Electrochem. Soc.* **2019**, *166*, A329.
[149] V. A. Nikitina, S. Y. Vassiliev, K. J. Stevenson, *Adv. Energy Mater.* **2020**, *10*, 1903933.
[150] A. J. Bard, L. R. Faulkner, *Electrochemical methods: fundamentals and applications*, 2nd ed., Wiley, Hoboken, NJ **2001**.
[151] J. H. Parker, J. J. Lowke, *Phys. Rev.* **1969**, *181*, 290.
[152] F. Hardcastle, I. Wachs, *Solid State Ion.* **1991**, *45*, 201.
[153] Y. S. Kim, V. Balland, B. Limoges, C. Costentin, *Phys. Chem. Chem. Phys.* **2017**, *19*, 17944.
[154] V. Srinivasan, J. Newman, *J. Electrochem. Soc.* **2004**, *151*, A1517.

[155] M. D. Levi, G. Salitra, B. Markovsky, H. Teller, D. Aurbach, U. Heider, L. Heider, *J. Electrochem. Soc.* **1999**, *146*, 1279.
[156] S. Yu. Vassiliev, E. E. Levin, V. A. Nikitina, *Electrochim. Acta* **2016**, *190*, 1087.
[157] S. Ardizzone, G. Fregonara, S. Trasatti, *Electrochim. Acta* **1990**, *35*, 263.
[158] H. Vogt, *Electrochim. Acta* **1994**, *39*, 1981.
[159] J. Duay, S. A. Sherrill, Z. Gui, E. Gillette, S. B. Lee, *ACS Nano* **2013**, *7*, 1200.
[160] L. Kong, C. Zhang, J. Wang, W. Qiao, L. Ling, D. Long, *ACS Nano* **2015**, *9*, 11200.
[161] C. Liu, E. I. Gillette, X. Chen, A. J. Pearse, A. C. Kozen, M. A. Schroeder, K. E. Gregorczyk, S. B. Lee, G. W. Rubloff, *Nat. Nanotech* **2014**, *9*, 1031.
[162] H.-S. Kim, J. B. Cook, H. Lin, J. S. Ko, S. H. Tolbert, V. Ozolins, B. Dunn, *Nat. Mater.* **2017**, *16*, 454.
[163] J.-Y. Shin, J. H. Joo, D. Samuelis, J. Maier, *Chem. Mater.* **2012**, *24*, 543.
[164] S. Zhang, G. Liu, W. Qiao, J. Wang, L. Ling, *J. Colloid Interface Sci.* **2020**, *562*, 193.
[165] Z. Liu, W. Dong, J. Wang, C. Dong, Y. Lin, I.-W. Chen, F. Huang, *iScience* **2020**, *23*, 100767.
[166] X. Zhai, J. Liu, Y. Zhao, C. Chen, X. Zhao, J. Li, H. Jin, *Appl. Surf. Sci.* **2020**, *499*, 143905.
[167] J. Ye, P. Shea, A. C. Baumgaertel, S. A. Bonev, M. M. Biener, M. Bagge-Hansen, Y. M. Wang, J. Biener, B. C. Wood, *Chem. Mater.* **2018**, *30*, 8871.
[168] D. Yan, A.-H. Lu, Z.-Y. Chen, L. He, W.-C. Li, *ACS Appl. Energy Mater.* **2021**, *4*, 1824.
[169] G. Wang, Y. Ling, Y. Li, *Nanoscale* **2012**, *4*, 6682.
[170] D. Lee, H. Lee, Y.-T. Kim, K. Lee, J. Choi, *Electrochim. Acta* **2020**, *330*, 135192.
[171] I. Andoni, J. M. Ziegler, G. Jha, C. A. Gadre, H. Flores-Zuleta, S. Dai, S. Qiao, M. Xu, V. T. Chen, X. Pan, R. M. Penner, *ACS Appl. Energy Mater.* **2021**, *4*, 6542.
[172] A. A. Lubimtsev, P. R. C. Kent, B. G. Sumpter, P. Ganesh, *J. Mater. Chem. A* **2013**, *1*, 14951.
[173] J. Meng, Q. He, L. Xu, X. Zhang, F. Liu, X. Wang, Q. Li, X. Xu, G. Zhang, C. Niu, Z. Xiao, Z. Liu, Z. Zhu, Y. Zhao, L. Mai, *Adv. Energy Mater.* **2019**, *9*, 1802695.
[174] C. Arrouvel, T. C. Peixoto, M. E. G. Valerio, S. C. Parker, *Comput. Theor. Chem.* **2015**, *1072*, 43.
[175] J. A. Yuwono, P. Burr, C. Galvin, A. Lennon, *ACS Appl. Mater. Interfaces* **2021**, *13*, 1791.
[176] H. Kaper, S. Sallard, I. Djerdj, M. Antonietti, B. M. Smarsly, *Chem. Mater.* **2010**, *22*, 3502.
[177] D. Fattakhova-Rohlfing, M. Wark, T. Brezesinski, B. M. Smarsly, J. Rathouský, *Adv. Funct. Mater.* **2007**, *17*, 123.
[178] J. Procházka, L. Kavan, M. Zukalová, O. Frank, M. Kalbáč, A. Zukal, M. Klementová, D. Carbone, M. Graetzel, *Chem. Mater.* **2009**, *21*, 1457.
[179] L. Kavan, M. Kalbáč, M. Zukalová, I. Exnar, V. Lorenzen, R. Nesper, M. Graetzel, *Chem. Mater.* **2004**, *16*, 477.
[180] X. Xin, X. Zhou, J. Wu, X. Yao, Z. Liu, *ACS Nano* **2012**, *6*, 11035.
[181] H. Han, T. Song, E.-K. Lee, A. Devadoss, Y. Jeon, J. Ha, Y.-C. Chung, Y.-M. Choi, Y.-G. Jung, U. Paik, *ACS Nano* **2012**, *6*, 8308.
[182] W. Li, F. Wang, S. Feng, J. Wang, Z. Sun, B. Li, Y. Li, J. Yang, A. A. Elzatahry, Y. Xia, D. Zhao, *J. Am. Chem. Soc.* **2013**, *135*, 18300.
[183] L. Bai, B. E. Conway, *J. Electrochem. Soc.* **1991**, *138*, 2897.
[184] L. Bai, B. E. Conway, *Electrochim. Acta* **1993**, *38*, 1803.
[185] M. D. Levi, D. Aurbach, In *Characterization of Materials* (Ed.: E. N. Kaufmann), John Wiley & Sons, Inc., Hoboken, NJ **2012**, p. com125.
[186] S. D. Kang, W. C. Chueh, *J. Electrochem. Soc.* **2021**, *168*, 120504.
[187] F. Walther, F. Strauss, X. Wu, B. Mogwitz, J. Hertle, J. Sann, M. Rohnke, T. Brezesinski, J. Janek, *Chem. Mater.* **2021**, *33*, 2110.
[188] A.-Y. Kim, F. Strauss, T. Bartsch, J. H. Teo, T. Hatsukade, A. Mazilkin, J. Janek, P. Hartmann, T. Brezesinski, *Chem. Mater.* **2019**, *31*, 9664.
[189] D. Weber, Đ. Tripković, K. Kretschmer, M. Bianchini, T. Brezesinski, *Eur. J. Inorg. Chem.* **2020**, *2020*, 3117.
[190] Y. Gao, J. Park, X. Liang, *J. Electrochem. Soc.* **2018**, *165*, A3871.
[191] A. Ulvestad, J. P. Mæhlen, M. Kirkengen, *ECS Trans.* **2015**, *64*, 107.
[192] S. Hildebrand, C. Vollmer, M. Winter, F. M. Schappacher, *J. Electrochem. Soc.* **2017**, *164*, A2190.
[193] Y. Cho, Y.-S. Lee, S.-A. Park, Y. Lee, J. Cho, *Electrochim. Acta* **2010**, *56*, 333.
[194] Y. Xu, X. Li, Z. Wang, H. Guo, B. Huang, *Mater. Lett.* **2015**, *143*, 151.
[195] Y. Yang, H. Zhu, F. Yang, F. Yang, D. Chen, Z. Wen, D. Wu, M. Ye, Y. Zhang, J. Zhao, Q. Liu, X. Lu, M. Gu, C. C. Li, W. He, *Nano Lett.* **2021**, *21*, 9675.
[196] Y. Ando, M. Okubo, A. Yamada, M. Otani, *Adv. Funct. Mater.* **2020**, *30*, 2000820.
[197] K. J. Griffith, Y. Harada, S. Egusa, R. M. Ribas, R. S. Monteiro, R. B. Von Dreele, A. K. Cheetham, R. J. Cava, C. P. Grey, J. B. Goodenough, *Chem. Mater.* **2021**, *33*, 4.

Wessel van den Bergh received his Ph.D. in Chemistry in 2022 from the University of South Carolina, USA. His research interests are focused on the use of controlled material design methodologies to study the relationship between material architecture and electrochemical behavior for energy storage applications. He will soon be a post-doctoral researcher at the Battery and Electrochemistry Laboratory (BELLA) at the Karlsruhe Institute of Technology (KIT), Germany.

Morgan Stefik is an Associate Professor in the Department of Chemistry and Biochemistry at the University of South Carolina and is the founding Director of the South Carolina SAXS Collaborative. He obtained his B.E. degree in Materials Engineering from California Polytechnic State University in 2005, and his Ph.D. degree in Materials Science from Cornell University in 2010. He then completed post-doctoral research at École Polytechnique Fédérale de Lausanne. Stefik's interests include nanomaterial synthesis, characterization, and fundamental energy device studies. Many of the research projects have a theme of seeking simplicity within a context of complexity.